AD NUMBER
AD358070
CLASSIFICATION CHANGES
TO: **UNCLASSIFIED**
FROM: **SECRET**
LIMITATION CHANGES
TO: **Approved for public release; distribution is unlimited.**
FROM: **Distribution authorized to DoD only; Administrative/Operational Use; 15 SEP 1960. Other requests shall be referred to Atomic Energy Commission (AEC), Washinton, DC. Pre-dates formal DoD distribution statements. Treat as DoD only. Formerly Restricted Data. NOFORN.**
AUTHORITY
DNA/SSTL ltr dtd 12 Jul 1995 DNA/SSTL ltr dtd 12 Jul 1995

DISCLAIMER NOTICE

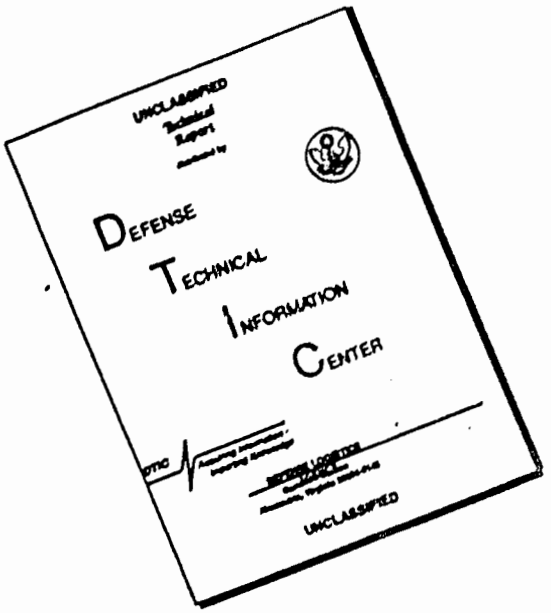

THIS DOCUMENT IS BEST QUALITY AVAILABLE. THE COPY FURNISHED TO DTIC CONTAINED A SIGNIFICANT NUMBER OF PAGES WHICH DO NOT REPRODUCE LEGIBLY.

SECRET

WT-1617

This document consists of 54 pages.

No. [redacted] of 180 copies, Series A

Operation

HARDTACK

April - October 1958

Project 1.12

GROUND-SHOCK SPECTRA from SURFACE BURSTS (U)

Issuance Date: September 15, 1960

HEADQUARTERS FIELD COMMAND
DEFENSE ATOMIC SUPPORT AGENCY
SANDIA BASE, ALBUQUERQUE, NEW MEXICO

FORMERLY RESTRICTED DATA

Handle as Restricted Data in foreign dissemination. Section 144b, Atomic Energy Act of 1954.

This material contains information affecting the national defense of the United States within the meaning of the espionage laws Title 18, U. S. C., Secs. 793 and 794, the transmission or revelation of which in any manner to an unauthorized person is prohibited by law.

SECRET

EXCLUDED FROM AUTOMATIC REGRADING; DOD DIR 5200.10 DOES NOT APPLY

SECRET

(18) AEC

(19)

(21) WT-1617

OPERATION HARDTACK — PROJECT 1.12 [43.

(6) GROUND-SHOCK SPECTRA from SURFACE BURSTS (U) (8)

(9) Final rept.,

(10) by J. F. Halsey, Project Officer
M. V. Barton,
J. M. Lindahl and
R. E. Hutton

(5) TRW Space Technology Laboratories, Inc.,
Los Angeles, California

Air Force Ballistic Missile Division
Air Research and Development Command
Inglewood, California

SECRET

FOREWORD

This report presents the final results of one of the projects participating in the military-effect programs of Operation Hardtack. Overall information about this and the other military-effect projects can be obtained from ITR–1660, the "Summary Report of the Commander, Task Unit 3." This technical summary includes: (1) tables listing each detonation with its yield, type, environment, meteorological conditions, etc.; (2) maps showing shot locations; (3) discussion of results by programs; (4) summaries of objectives, procedures, results, etc., for all projects; and (5) a listing of project reports for the military-effect programs.

ABSTRACT

Self-contained mechanical reed gages, capable of measuring the displacement-shock spectrum over a frequency range of 3 to 300 cps in any one direction, were used during Shots Cactus and Koa. Canisters containing the gages were normally placed with their tops flush to the ground level at predicted pressure levels from 75 to 200 psi on both shots. Additional gages were installed in earth-confined arch structures of Project 3.2. Satisfactory records were obtained for both shots.

Limited comparisons have been made between the results obtained for the low-yield (Cactus) and high-yield (Koa) shots at the Eniwetok Proving Ground (EPG) and between the results for Shot Cactus and the low-yield Shots Whitney, Galileo, and Smoky during Operation Plumbbob at the Nevada Test Site (NTS).

In general, vertical and radial displacements for Shot Koa were much lower than expected from the extrapolation of data obtained from low-yield shots during Operation Plumbbob. Differences in soil conditions, surface versus raised bursts, and topography variations may have been contributing factors. The Appendix contains the preliminary results of intensive parametric analyses and theoretical studies being made in an attempt to establish suitable scaling laws.

In general, the vertical displacements at low frequencies (less than 10 cps) are lower and the displacements at high frequencies (greater than 100 cps) are higher from Shots Cactus and Koa than from the shots during Operation Plumbbob. Also, the ratios between radial and vertical components at various ranges tend to be more nearly equal for the two Hardtack shots than for the Plumbbob shots. Specifically, at 110 psi the vertical displacements of Shot Cactus were significantly less (one third to one fifth) than for the Plumbbob shots up to 20 cps where they are almost equal. Above 50 cps, the vertical displacements for Shot Cactus were two to four times greater than for the Plumbbob shots. The radial displacements at 110 psi for Shot Cactus were about the same as for the Plumbbob shots up to 10 cps and two to four times greater at higher frequencies.

A comparison of the vertical displacements at 90 psi for Cactus and at 84 psi for Koa, shows that the displacements for Koa were higher in the low-frequency range (twice as high at 3 cps), lower for the intermediate-frequency range (10 to 50 cps), and about equal for the high-frequency range. The radial displacements for Cactus at 90 psi were about the same as for Koa at 84 psi, except in an intermediate-frequency range (10 to 50 cps) where the Cactus values were found to be greater.

CONTENTS

FIGURES

GROUND-SHOCK SPECTRA from SURFACE BURSTS

OBJECTIVE

The objective was to measure directly the displacement-shock spectra, near the ground surface, of air-induced and ground-transmitted ground shocks produced by the blast wave from surface-burst nuclear detonations. The displacement-shock spectrum is a plot of peak displacement of a set of several linear fixed-frequency oscillators (of single degree of freedom) to specific blast wave, as a function of the frequency of the oscillators. Velocity- and acceleration-shock spectra are derived from the measured displacement-shock spectra. The measurements do not correspond to the ground motions but are the responses of linear vibration systems relative to the ground motion.

BACKGROUND

Headquarters, U.S. Air Force, has required the Air Force Ballistic Missile Division (AFBMD), Air Research and Development Command (ARDC), to provide data for a "hard" operational base for one of the ICBM missile systems. The AFBMD, in conjunction with the Space Technology Laboratories, Inc. (STL), formerly a division of The Ramo-Wooldridge Corporation (R-W), will specify input data to architect-engineer firms. As a minimum, the environmental information includes vertical and radial ground-shock spectra, permanent ground displacements, and levels of nuclear and thermal radiation. Desirable information includes soil pressures and transient ground displacements and acceleration.

The Air Force Special Weapons Center (AFSWC) furnished to AFBMD the best-known limits of peak values and transient variations of ground accelerations and displacements for the required overpressure region, based on measurements made by Sandia Corporation (SC), Stanford Research Institute (SRI), and Ballistic Research Laboratories (BRL) during operations prior to Plumbbob.

For the measurements of accelerations and displacements during Operation Plumbbob, SC, SRI, and BRL used what might be termed "standard acceleration and displacement instrumentation"; AFBMD/R-W used, for the first time in the weapon-effect tests, self-contained sets of single-frequency reed gages for direct determination of the displacement-shock spectrum. The measurements provided a better understanding of the ground-shock phenomena for kiloton-range devices. On the other hand, the shock-spectra data could not be extrapolated into the high-yield range because of the lack of normal acceleration-time records for the megaton-range devices.

The results of the AFBMD/R-W measurements during Operation Plumbbob are contained in Reference 1.

It was considered desirable to establish scaling laws for effects at different yields, particularly for application to missiles, which possess very low natural frequencies. The first attempt at scaling was made on the basis that the displacement shock at zero frequency (the peak ground displacement at the surface) should be proportional to the total overpressure impulse. Because displacement-shock spectra were not measured below 3 cps during Operation Plumbbob, the correlation at zero frequency could not be made. The attempt at correlation at 3 cps indicated a trend, but the results were indecisive. As shown in Figure 1, the least scatter of data appears to be given by a plot of vertical displacement at 3 cps versus $(\text{overpressure})^{1/6}$ $(\text{yield})^{1/3}$.

Figure 2 shows a composite plot of pertinent Plumbbob results for the vertical direction. Similarly, Figure 3 shows a composite plot of Plumbbob results for the radial direction.

Participation during Operation Hardtack was a continuation of the Plumbbob effort. Shot Cactus was in the kiloton range, and Shot Koa was in the megaton range. Correlation is available to a limited extent between low yields and high yields at the EPG, and between low yields

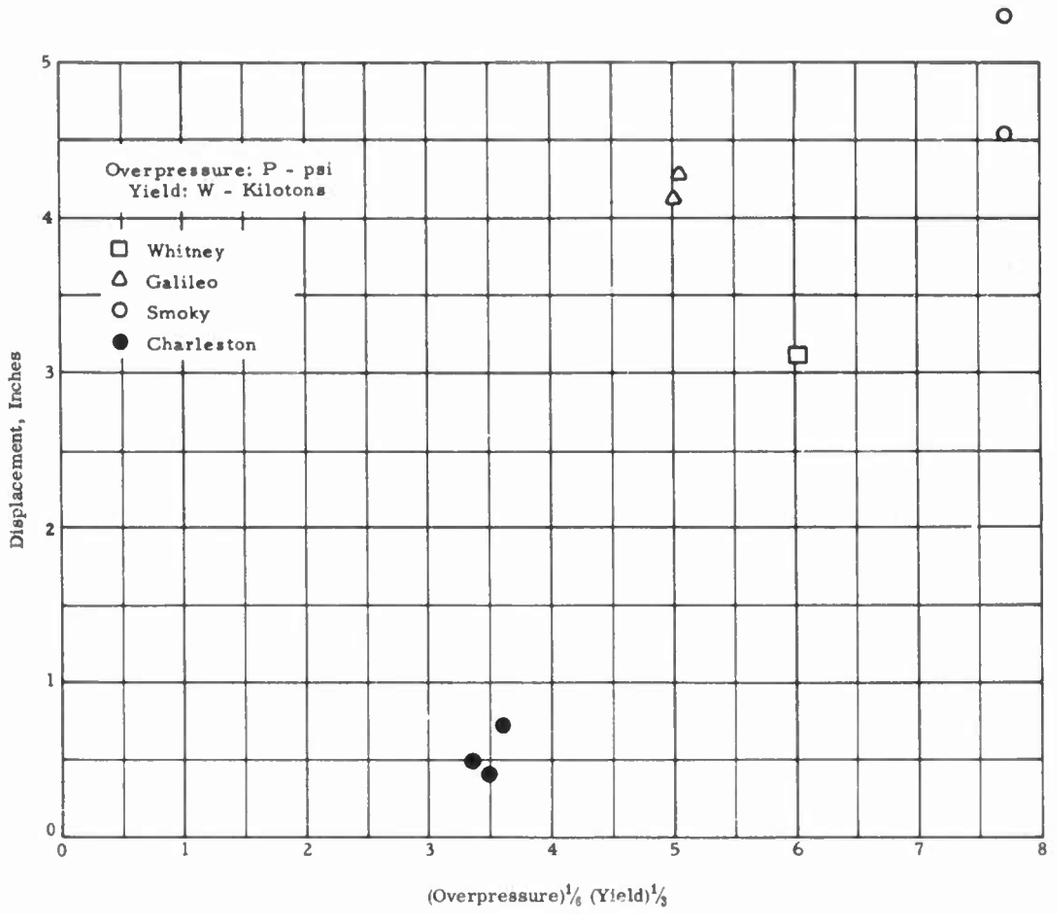

Figure 1 Displacement at 3 cps versus vertical direction.

at the EPG and the NTS, which permits scaling of surface ground-shock spectra with yield for similar conglomerate soils.

The shock spectra can be used for making estimates of upper bounds of response of missiles and structures subjected to ground motions, for conditions similar to those under which the shock spectra are obtained. The structures considered are, in general, linear with small damping, although some effort is under way to extend methods to simple nonlinear structures.

Specifically, the shock spectra are useful for estimations of: (1) maximum stress, displacement, or acceleration induced in a structure; (2) design criterion for a supporting-structure shock mounting which will protect the missile; and (3) shock environment for equipment attached to the missile.

THEORY

Complete discussions of the theory and application of shock spectra are given in References 2, 4, and 7. Briefly, if a shock due to ground motions is applied to a linear structure attached

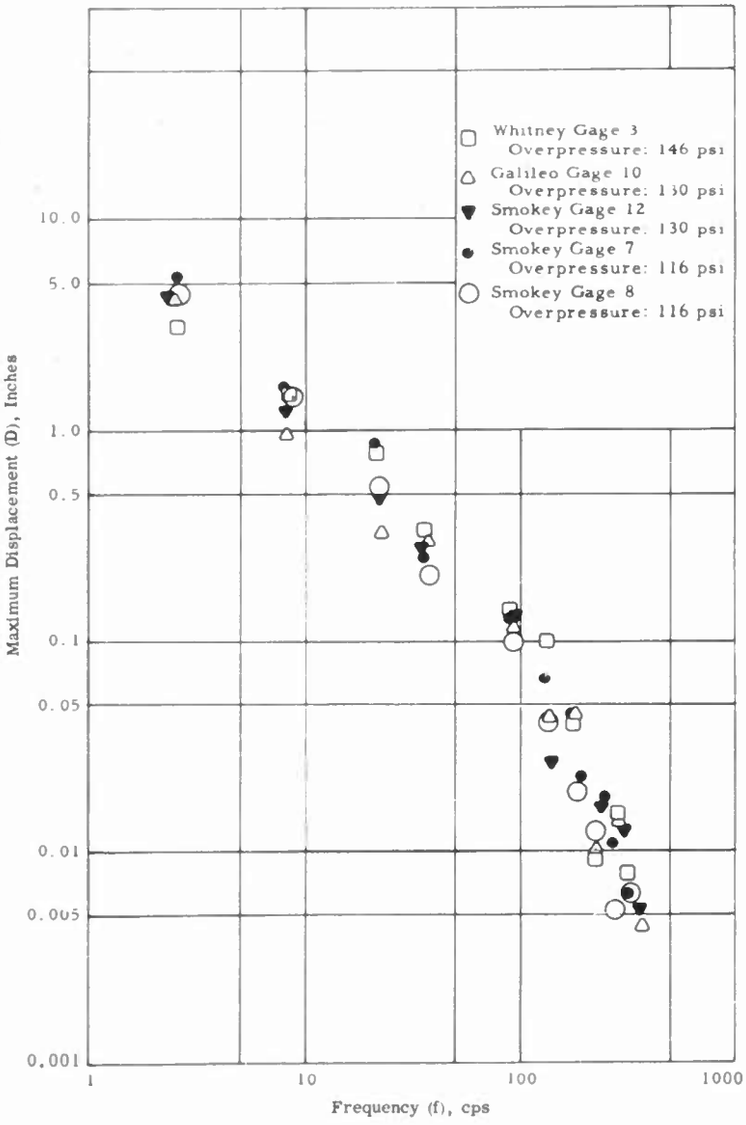

Figure 2 Displacement shock spectrum, vertical direction.

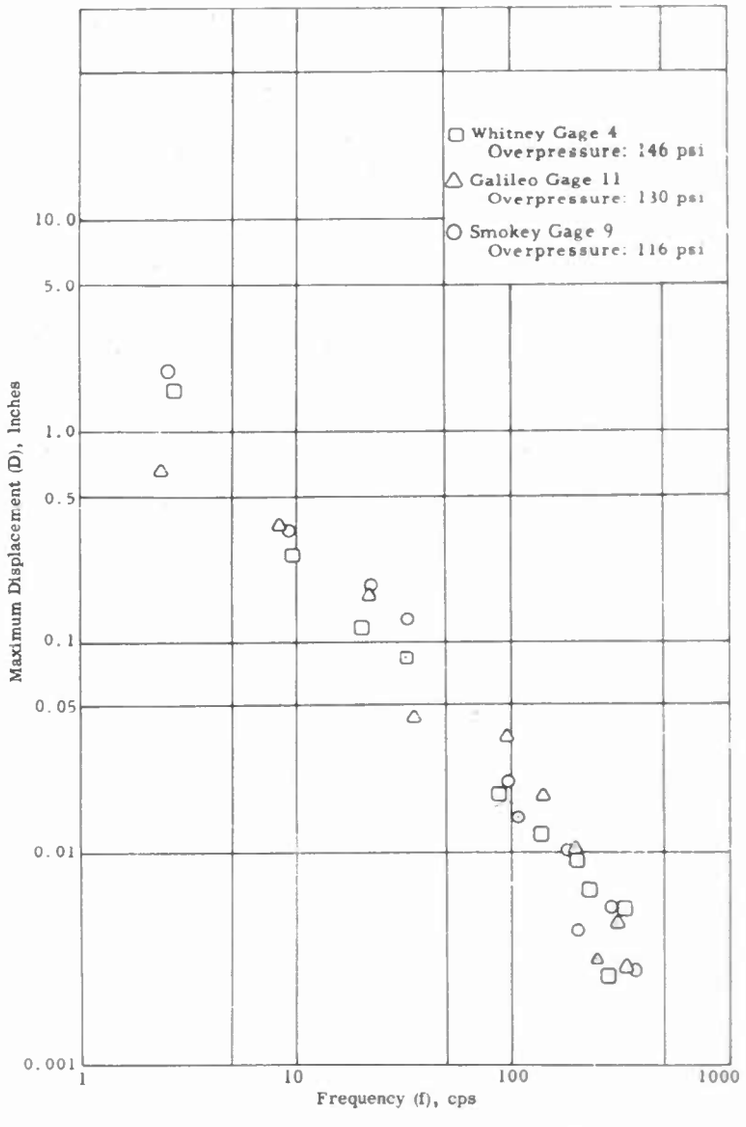

Figure 3 Displacement shock spectrum, radial direction.

to the ground, the displacement of any point of the structure relative to the ground can be expressed as a sum of principal mode responses:

$$u(t,x,y,z) = \Sigma q(t)\,\phi(x,y,z) \tag{1}$$

Where: $u(t)$ = displacement relative to ground
$q(t)$ = generalized coordinate
$\phi(x,y,z)$ = mode shape

An upper bound of response is obtained assuming all modes have reached their peak values at the same time:

$$u \leq \Sigma \left| q_{max}\,\phi \right| \tag{2}$$

For an acceleration input, it can be shown (Reference 4) that for each mode:

$$\ddot{q} + 2\epsilon\omega\dot{q} + \omega^2 q = -\gamma a(t) \tag{3}$$

Where: q = generalized displacement relative to ground
ω = frequency of mode
ϵ = ratio of damping to critical viscous damping
γ = kinematic factor = $\int \rho\,\phi\,dv / \int \rho\,\phi^2\,dv$
ρ = mass distribution per unit volume
$a(t)$ = acceleration of ground as function of time

The solution to Equation 3 for small damping is

$$q_{max}(\omega,\epsilon) = \max_{t \to 0} \left| \frac{\gamma}{\omega} \int_0^t a(\tau) e^{-\epsilon\omega(t-\tau)} \sin \omega(t-\tau)\,d\tau \right| \tag{4}$$

Assuming an idealized single-degree-of-freedom system, such as a point mass on a weightless cantilever spring, the equation of motion for the mass is

$$\ddot{Q} + 2\epsilon\omega\dot{Q} + \omega^2 Q = -a(t) \tag{5}$$

With an appropriate gage factor to adjust for stylus position and for the fact that the sets of cantilevered mass systems have distributed mass, the reed shock gages will give direct readings of peak displacements as solutions of Equation 5. The frequency spectrum of the peak displacements of the masses relative to the base that is being accelerated is called the displacement-shock spectrum, which is defined as:

$$D(\omega) = Q_{max} = \max_{t \to 0} \left| \frac{1}{\omega} \int_0^t a(\tau) e^{-\epsilon\omega(t-\tau)} \sin \omega(t-\tau)\,d\tau \right| \tag{6}$$

If the displacement spectrum, $D(\omega)$, is known, the modal response of any other structure having the same damping as the gage is given by:

$$q_{max} = \gamma D \tag{7}$$

or the upper bound of response by (from Equation 2):

$$u \leq \Sigma \left| \gamma D \phi \right| \tag{8}$$

The "velocity" shock spectrum is defined as

$$V = \omega D \tag{9}$$

This quantity has the dimensions of velocity, but is not the peak velocity of the mass relative to the base. The velocity shock spectrum is useful, however, in the determination of an upper bound of strain energy in the structures and is discussed in Reference 7.

The acceleration shock spectrum is defined as

$$A = \omega^2 D \tag{10}$$

and can be shown to be (Reference 7), the peak absolute acceleration of the mass for small damping, namely:

$$A = \max \left| \ddot{Q} + a \right| \tag{11}$$

Plumbbob results indicated a possible correlation of shock spectra (a particular displacement for a particular frequency) with the total ground impulse (air slap) resulting from that particular (low-yield) air-overpressure wave form. Predicted curves were derived on the basis that the rise time (free-air overpressure versus time) from a high-yield detonation was similar, if not identical, to that from a low-yield detonation, but that the duration (total impulse) was longer. This increase in duration obtains greater displacements for high-yield nuclear devices at low frequencies, with practically no change of the same measurement at high frequencies for this type of device.

For a better determination of how yield, pressure, depth, and soil parameters affect the scaling of measured shock spectra to different explosions and different sites, a separate study to create a mathematical model that would estimate the gross effects of these parameters has been initiated. Although this study has not been completed, a brief outline of the work, published as Reference 8, is given in the Appendix.

OPERATIONS

Activities at the test site included the placement of instruments, recovery of record plates and, where possible, recovery of instruments. Recovery of record plates from instruments inside two of the Project 3.2 test structures was not immediately possible, because the structures had been damaged by the blast effects of Shot Koa. Recovery of these record plates was accomplished in October 1958, by Project 3.2 personnel.

The records of two other instruments, L8 and L9, Station 125.05, for Shot Koa were invalidated by the unexplained formation of a crater, 30 feet in diameter and 10 feet deep. One of these two instruments had been displaced from its original position in the ground to a position approximately 10 feet away on top of the crater lip.

Two types of gages were used. Both were self-contained mechanical units requiring no electronic or communication channels.

INSTRUMENTATION: HIGH-FREQUENCY GAGE

The high-frequency gage (120 pounds) consists of ten cantilevered masses mounted on a common base plate as shown in Figure 4. The natural frequencies of the cantilevered-mass systems are approximately 3, 10, 20, 40, 80, 120, 160, 200, 250, and 300 cps. (For Shot Koa, however, certain of the 3-cps and 10-cps cantilevered masses were immobilized, because the large displacements anticipated could not be recorded on the area available on the record plate.) Peak responses to shock input for each cantilevered-mass system were recorded on polished, smoked, stainless-steel record plates by the movement of a stylus attached to each mass. The length of the marks (measure of displacement) was determined by use of a microscopic micrometer in the laboratory.

Protection for the gage was obtained by placement inside a cylindrical canister (430 pounds, 2 feet in diameter, and 2 feet deep). Transmission of shock input to the gage, either in the vertical or horizontal (radial) direction, was secured by bolting the gage in the desired position to the 1-inch-thick base plate. Figure 5 shows a canister (lid off) with a gage installed in the vertical position.

A spring-driven record-preserving mechanism was built into the gage to raise the original record $\frac{1}{4}$ inch, preventing subsequent shock inputs from invalidating the original record. A

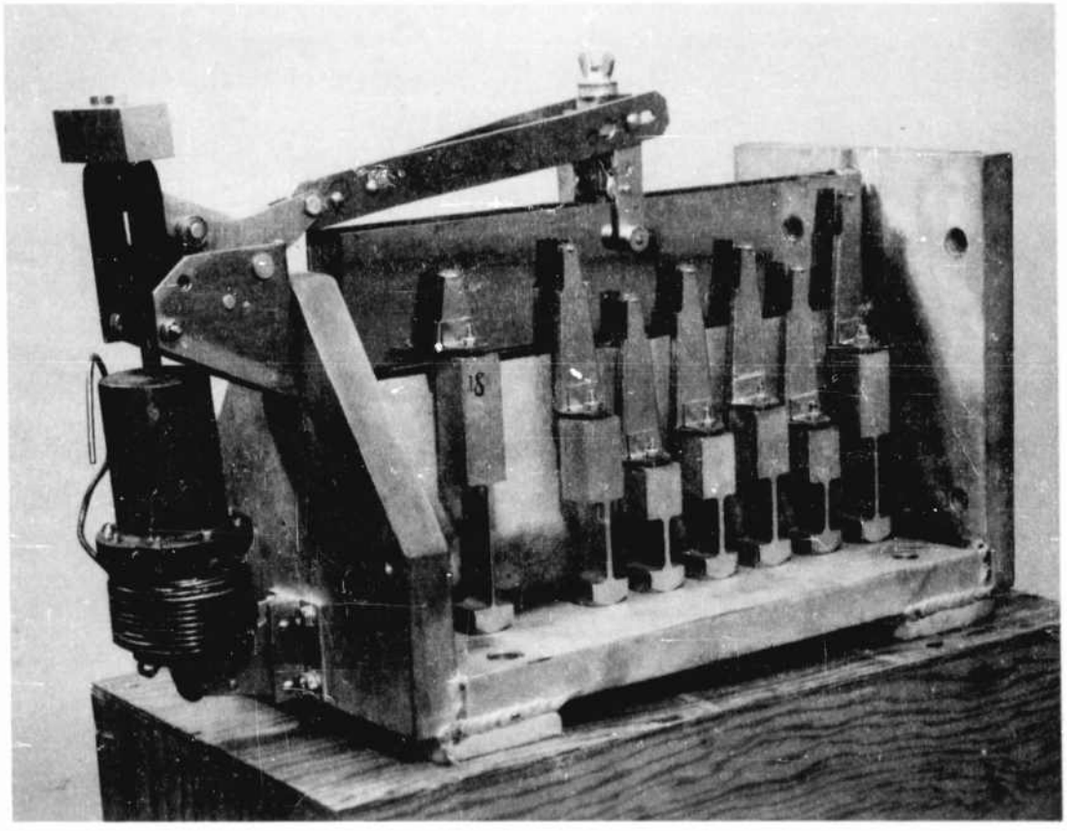

Figure 4 High-frequency gage.

comparison of the record-plate vertical positions before and after the initial shock input may be made by inspection of Figures 4 and 6. The time interval for the initiation of the record-plate movement was approximately 5 minutes.

INSTRUMENTATION: LOW-FREQUENCY GAGE

The low-frequency gage (40 pounds) had three guide-tube assemblies containing roller-mounted bob weights elastically restrained by tension springs pulling on either end of the bob weight. The three assemblies possessed natural frequencies of 3, 6, and 10 cps. Each bob weight had a needle stylus which scribed through a slot in the guide tube onto a smoked metal record surface that was outside the guide tube.

A spring-driven record-preserving mechanism locked the bob weights after approximately a 5-minute delay from the time of the initial shock input. As with the high-frequency gages, the lockout mechanism was employed to prevent subsequent shock inputs from invalidating the original record.

Protection for the gage was obtained by placement inside a cylindrical canister (160 pounds,

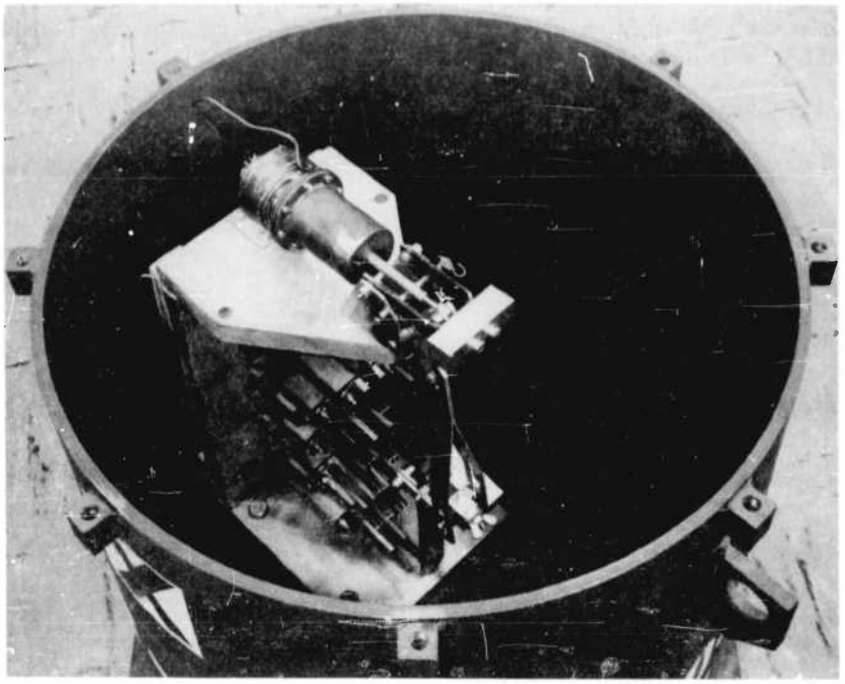

Figure 5 High-frequency gage installed in vertical position in canister.

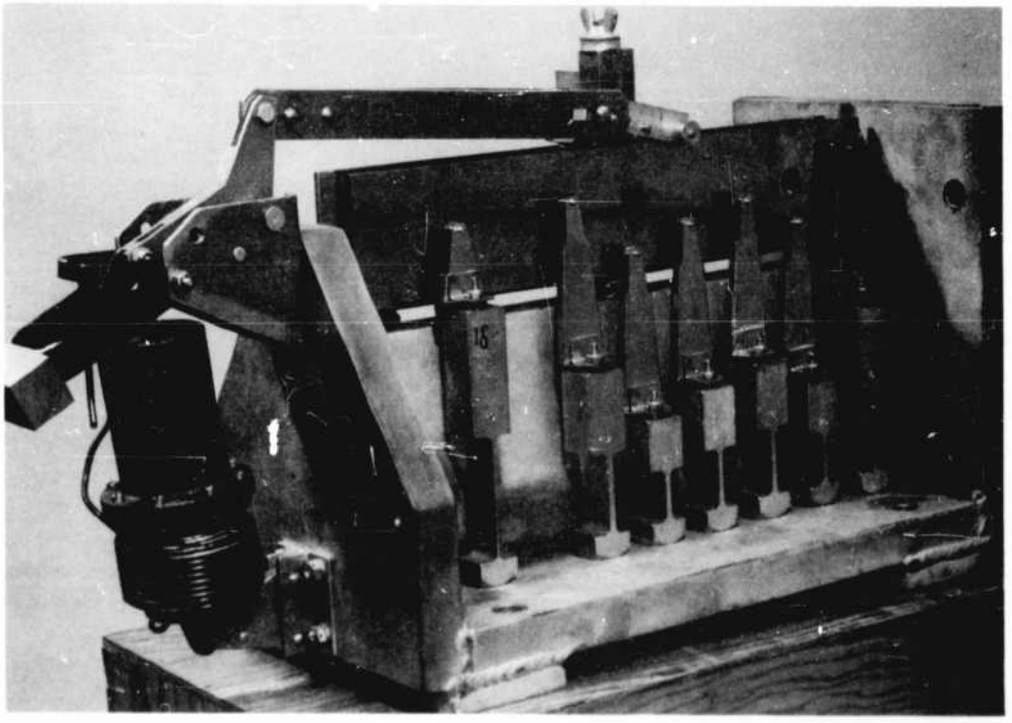

Figure 6 High-frequency gage. Record plate is in raised position.

8 inches in diameter and approximately 5 feet long). Figure 7 shows a gage assembly partially inserted into the canister.

GAGE INSTALLATIONS

Figures 8 and 9 show the location and layout of the project installations for Shots Cactus and Koa.

The sequence of installation of gages when used for measurements in the free field was:

1. Excavation of 30-inch cubical holes for the canisters with the high-frequency gages. Excavation of 1-foot-diameter holes, 5 feet deep, for vertical installation, and 1-foot-deep holes,

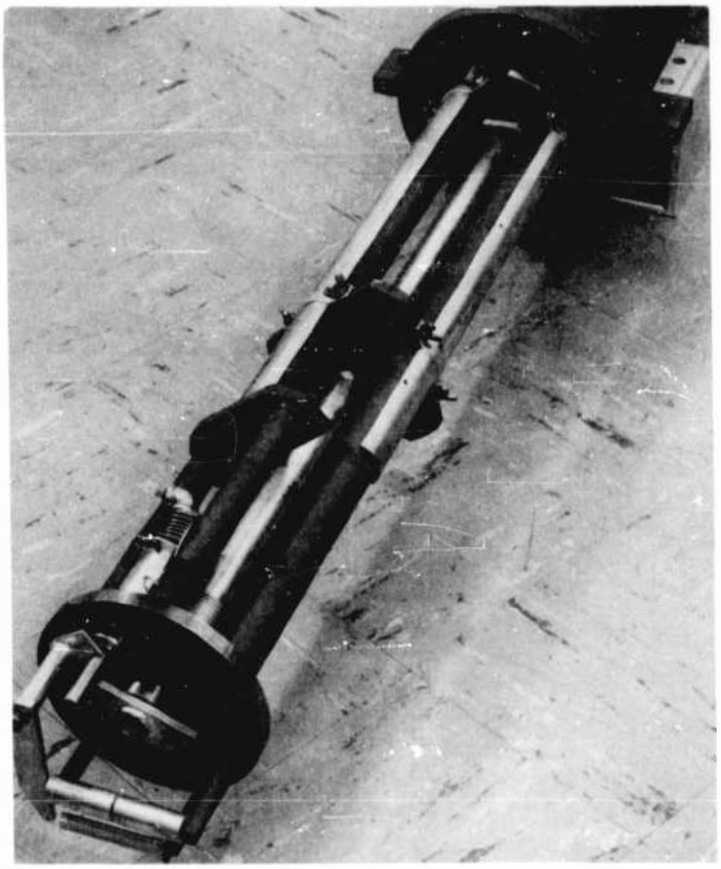

Figure 7 Low-frequency gage
partially inserted into canister.

5 feet long, for radial installation of canisters with low-frequency gages. The object was to have the tops of the canisters flush with the surrounding ground.

2. Placement of canisters, as shown in Figures 10, 11, 12, and 13.
3. Backfilling around canisters, with native material. Compaction was obtained through the use of water and hand tamping. It is estimated that a compaction of 90 percent of maximum density at optimum moisture content was obtained.
4. Placement of smoked record plates in the high-frequency gages. The low-frequency record plates were installed as a part of the low-frequency gage assemblies.
5. Cocking of record-preserving mechanism.
6. Careful placement and bolting of canister lids. (Rough handling could excite the gages.)
7. Placement of two layers of sandbags (each 4 to 5 inches thick) over the lids.

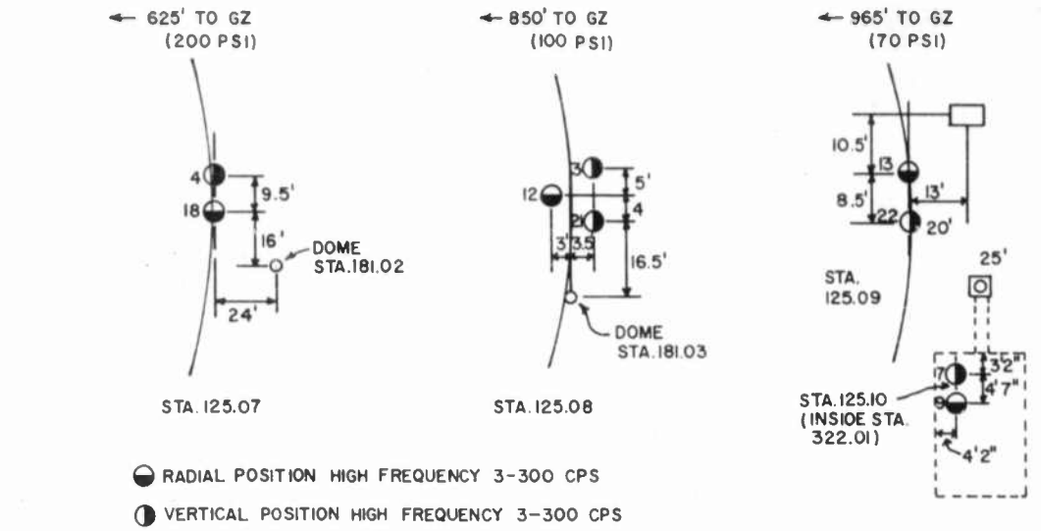

Figure 8 Gage layout, Site Yvonne, Shot Cactus.

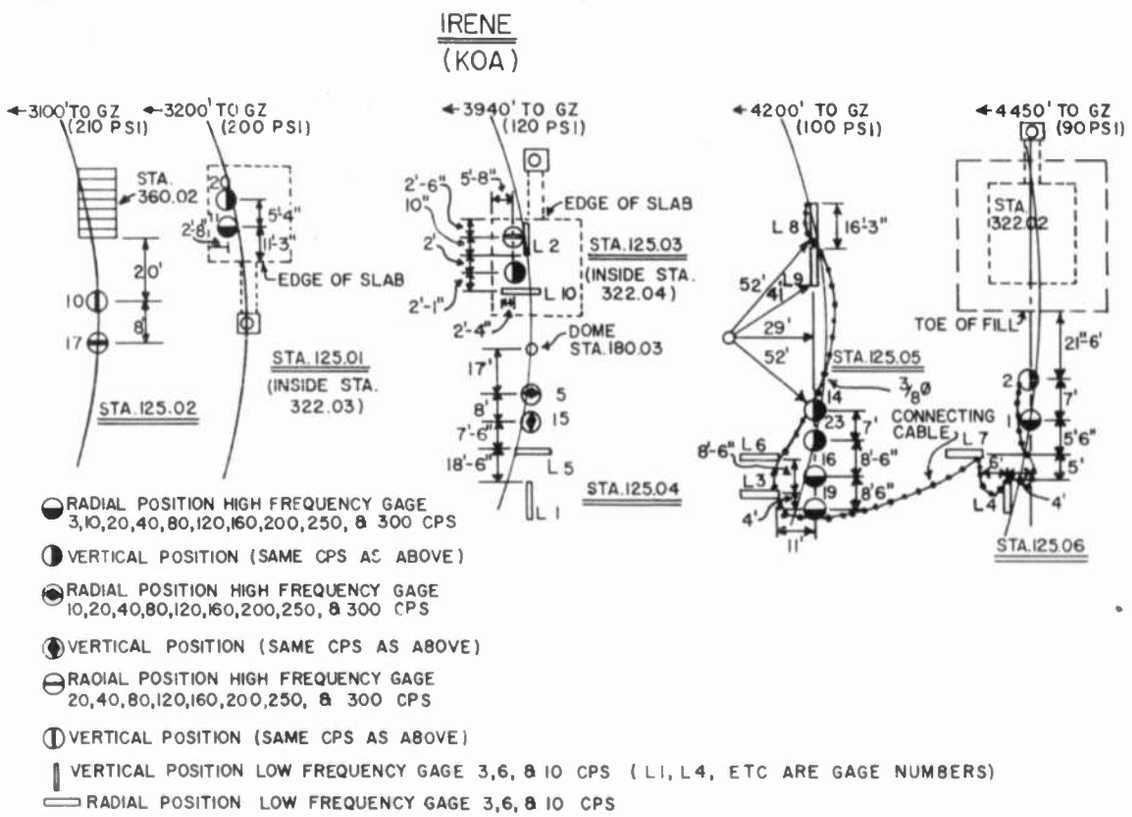

Figure 9 Gage layout, Site Irene, Shot Koa.

Figure 10 Station 125.09, Site Yvonne.
Placement of high-frequency gage canister.

Figure 11 Station 125.09, Site Yvonne.
High-frequency gages.

Figure 12 Station 125.08, Site Yvonne.
High-frequency gages in place.

Figure 13 Station 125.05, Site Irene.
Low-frequency gages in foreground.

The installation within the Project 3.2 structures required the early placement of six canisters for high-frequency gages (not containing gages and record plates) inside these structures (two canisters each in Stations 322.01, 322.03, and 322.04), because the dimensions of the canisters did not permit their passage through the finished hatches of these structures. Each canister was bolted to the floor slab with four $\frac{3}{4}$-inch anchor bolts. Gage and record-plate installation, and cocking of the record-preserving mechanism, were accomplished later. The low-frequency instruments were placed inside the finished structure (Station 322.04) and anchored to the floor slabs with $\frac{3}{4}$-inch anchor bolts. The gage in the vertical position was guyed with

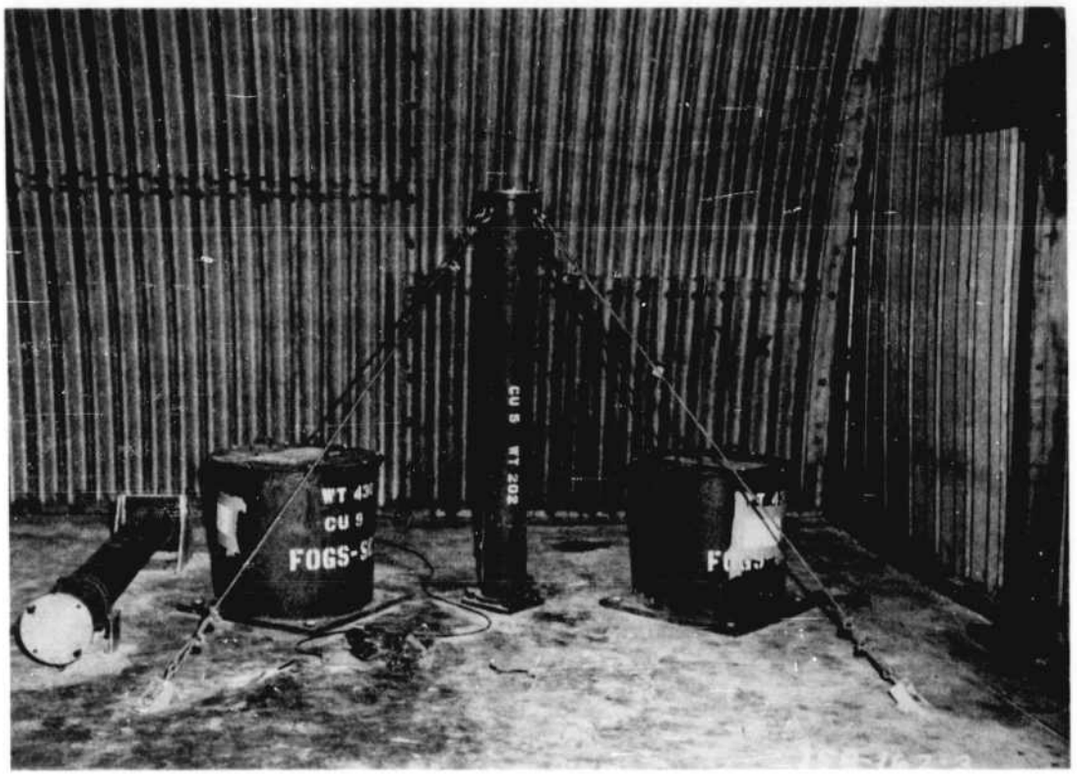

Figure 14 Station 125.03, Site Irene.
Canister installation inside Station 322.04.

four lengths of $\frac{3}{8}$-inch aircraft cable. Figure 14 shows the canister installation inside Station 322.04.

GAGE CALIBRATION

The calibration consisted of making three measurements on each gage: (1) the natural frequency of each reed, (2) the effective viscous damping ratio, and (3) a geometric parameter, denoted by the gage factor G. This geometric factor is required because the length of the trace that is recorded on the record plate is dependent upon the location of the scribe on the vibrating reed and the mass distribution.

High-Frequency Gages. The fundamental natural frequency for each reed-mass system was determined by placing each gage on a shake table and reading, by means of a Berkley counter, the lowest frequency that produced resonance of each cantilever mass.

The damping ratio was obtained by fastening a small crystal accelerometer to a reed, displacing the reed, and recording the decay motion on a Helland recorder, during which time the scribe was in contact with the record plate. Because the damping varied slightly with needle

pressure and with the amplitude of motion, the test was not performed on each of the gages but only on a sample, to get typical values of the viscous damping ratio. This test also gave a natural frequency of each reed on the gages tested and was used as a check on the shake tests.

A gage factor for each typical cantilevered-mass system was computed or obtained experimentally. This gage factor is a multiplying factor for converting the length of the trace on the record plate to an equivalent displacement of a point mass, or:

$$D = GS \tag{12}$$

Where: D = displacement of point mass
G = gage factor
S = length of trace made by stylus

For one mode:

$$S = q_{max}\phi(s) \tag{13}$$

Where: $\phi(s)$ = mode value at stylus

or since $q_{max} = \gamma D$ (from Equations 4 and 6)

$$S = \gamma D \phi(s) \tag{14}$$

Hence, from Equations 14 and 12,

$$G = 1/\gamma \phi(s) \tag{15}$$

Now $\gamma \phi(s)$ can be determined experimentally by applying a known constant acceleration and measuring the stylus trace. From Equation 3, the value of q for constant applied acceleration c is

$$q_c = \gamma c/\omega^2 \tag{16}$$

and the length of the stylus trace is

$$U = q_c \phi(s) = \frac{\gamma c}{\omega^2} \phi(s)$$

or

$$G = 1/\gamma \phi(s) = c/U\omega^2 \tag{17}$$

Where: c = constant acceleration
U = length of trace
ω = frequency of reed-mass system

For the lowest-frequency reeds, the static deflection U was measured by applying a 1-g load by inserting the record, turning the gage on end, and removing the record. For the intermediate-range reeds, a larger load was required. A steady 15-g load was applied by placing the gages in a centrifuge, bringing the centrifuge up to speed slowly, and then stopping the centrifuge. The trace recorded corresponded to the 15-g applied load. For the highest-frequency reeds, a higher load was required. Since the centrifuge capacity was limited to approximately 15-g for the 120-pound gages, the G values for the highest-frequency reeds were determined from calculations using Equation 15.

Low-Frequency Gages. The natural frequency was measured by displacing the bob weight and letting it interrupt a light beam as the weight vibrated under free vibrations. The light beam was focused on a solar battery. The output voltage of the solar battery was amplified by a dc amplifier and fed into a Berkley meter. The Berkley meter measured the length of time between the variations in the voltage caused by the interruption of the light beam. This period of time corresponded to the natural frequency.

The damping ratio was measured by displacing the bob weight, recording the motion on the record plate, and manually rotating the plate during the decay motion of the weight; successive amplitudes could be detected and hence the damping ratio determined.

The G value of these gages could be determined by applying a load of 1-g and measuring the static deflection at the scribe. However, in this system, which closely approximates a single degree of freedom, the G value can be shown to be very nearly 1.0.

DATA REQUIREMENTS

The specification of design parameters and the cross-corroboration between low-yield and high-yield devices required that the displacement-shock spectra be obtained for the preselected overpressure level of 100 psi. Statistical considerations, variable ground conditions, and a probable variation in yield suggested the placement of gages in overpressure regions varying from below 100 psi to above 100 psi on both Shots Cactus and Koa. Accordingly, the gages were placed as shown in Figures 8 and 9.

The desire to delineate the attenuation of the ground shock through depth, and thence through an elastic floor slab, led to the placement of gages within the Project 3.2 structures.

Free-air overpressures were furnished by Project 1.7.

DISCUSSION AND RESULTS

The results are given in Tables 1 through 9 and Figures 16 through 44.

Of primary interest are the comparison and correlations between the results obtained for: (1) high-yield (Koa) and low-yield (Cactus) shots for similar soils and topography at EPG and (2) similar yields for different soils and topography (Shot Cactus at EPG and Shots Whitney, Galileo, and Smoky during Operation Plumbbob at NTS).

The following general trends were established for free-field shock-spectrum displacements near the surface at similar overpressures:

1. The vertical displacements at low frequencies (less than 10 cps) are less for EPG than for NTS, regardless of yield. Preliminary scaling of Plumbbob data, shown as Figure 15, indicated that the high-yield shot (Koa) should have given about three times the displacement of the low-yield Plumbbob shots if the soil conditions were similar. The much higher seismic velocity at EPG may qualitatively explain the differences. Quantitative studies are now being performed to establish scaling relationships to take into account soil factors. As mentioned earlier, the preliminary results of these studies are shown in the Appendix of this report.
2. The vertical and radial displacements at high frequencies (greater than 100 cps) are greater at EPG than NTS, regardless of yield. Differences in seismic velocity may also be a factor in this case.
3. The vertical and radial components at the low- and high-frequency ends of the spectrum are nearly equal for the low-yield shot (Cactus) at EPG. At NTS, the vertical component is about three times the radial component.

Shot Cactus. The vertical displacements measured by two gages adjacent to each other (21 and 3, Station 125.08) at 110 psi overpressure are similar (probably within 15 percent) as shown in Figures 18 and 19.

The vertical displacements at 110 and 90 psi (Gages 21 and 3, Station 125.08, and Gage 22, Station 125.09) show a local peaking at about 40 cps (Figures 18, 19, and 21).

At 110 psi (Station 125.08) the radial components (Gage 12) are only slightly lower (within 25

TABLE 1 DISPLACEMENT SHOCK SPECTRUM, SHOT CACTUS, SURFACE, VERTICAL DIRECTION

Station	125.07	Station	125.08	Station	125.09
Overpressure	210 psi	Overpressure	110 psi	Overpressure	90 psi
Range	625 ft.	Range	850 ft.	Range	965 ft.
Gage Number	4	Gage Number 3		Gage Number 21	Gage Number 22
f, cps	D, inches	f, cps	D, inches	f, cps	D, inches	f, cps	D, inches
3.3	—	3.0	1.414	2.9	1.751	3.2	1.335
9.9	0.920	9.7	0.640	10.0	0.550	9.5	1.094
23.0	0.653	23.0	0.488	23.0	0.508	23.0	0.607
51.0	0.657	48.0	0.697	49.0	0.584	49.0	0.605
91.0	0.339	90.0	0.295	90.0	0.293	89.0	0.201
138	0.251	138	0.096	136	0.106	137	0.082
181	0.155	181	0.066	182	0.043	180	0.043
221	0.123	213	0.058	220	0.033	220	0.017
262	0.093	250	0.042	256	0.021	247	0.004
288	0.085	286	0.023	288	0.015	290	0.007

TABLE 2 DISPLACEMENT SHOCK SPECTRUM, SHOT CACTUS, SURFACE, RADIAL DIRECTION

Station	125.07	Station	125.08	Station	125.09
Overpressure	210 psi	Overpressure	110 psi	Overpressure	90 psi
Range	625 ft.	Range	850 ft.	Range	965 ft.
Gage Number	18	Gage Number	12	Gage Number	13
f, cps	D, inches	f, cps	D, inches	f, cps	D, inches
3.0	1.772	2.9	1.159	3.1	0.954
10.6	0.688	10.3	0.409	9.8	0.478
23.0	0.614	23.0	0.308	23.0	0.341
49.0	0.365	48.0	0.225	48.0	0.197
91.0	0.155	90.0	—	90.0	0.054
138	0.027	137	0.073	138	0.034
181	0.094	180	0.053	181	0.022
220	0.046	215	0.036	219	0.020
264	0.038	262	0.029	251	0.013
283	0.027	289	0.022	288	0.011

TABLE 3 DISPLACEMENT SHOCK SPECTRUM, SHOT CACTUS, INSIDE SHELTER

Vertical Direction		Radial Direction	
Station	125.10	Station	125.10
Overpressure	90 psi	Overpressure	90 psi
Range	965 ft.	Range	965 ft.
Gage Number	7	Gage Number	9
f, cps	D, inches	f, cps	D, inches
2.9	1.424	3.0	1.099
9.5	0.865	9.7	0.404
23.0	0.233	23.0	0.163
48.0	0.091	28.0	0.026
90.0	0.015	91.0	0.008
138	0.011	138	0.005
182	0.004	180	0.003
216	0.003	219	0.001
262	0.003	263	0.002
281	0.003	288	0.002

TABLE 4 DISPLACEMENT SHOCK SPECTRUM, SHOT KOA, SURFACE, VERTICAL DIRECTION

Station 125.02 Overpressure 196 psi Range 3,100 ft. Gage Number 10 High Frequency		Gage Number 1 Low Frequency		Station 125.04 Overpressure 86 psi Range 3,940 ft. Gage Number 15 High Frequency		Gage Number 14 High Frequency		Station 125.05 Overpressure 84 psi Range 4,200 ft. Gage Number 23 High Frequency	
f, cps	D, inches	f, cps	D, inches	f, cps	D, inches	f, cps	D, inches	f, cps	D, inches
3.1	1.138	2.7	2.667	3.0	—	3.1	2.985	3.0	2.659
10.6	0.305	5.3	1.836	10.0	1.019	9.4	0.686	9.7	0.583
23.0	1.142	8.8	0.818	22.0	0.797	23.0	0.520	23.0	0.619
48.0	0.888			49.0	0.539	49.0	0.395	51.0	0.292
87.0	0.259			90.0	0.220	88.0	0.151	86.0	0.171
138	0.185			136	0.111	137	0.031	138	0.088
180	0.122			178	0.064	181	0.030	180	0.028
218	0.082			218	0.044	214	0.033	220	0.030
263	0.051			258	0.041	250	0.015	260	0.014
289	0.019			287	0.030	288	0.019	284	0.011

TABLE 5 DISPLACEMENT SHOCK SPECTRUM, SHOT KOA, SURFACE, VERTICAL DIRECTION

Station 125.06 Overpressure 78 psi Range 4,450 ft. Gage Number 4 Low Frequency		Gage Number 2 High Frequency	
f, cps	D, inches	f, cps	D, inches
2.8	1.935	2.9	2.439
5.1	1.328	10.3	0.423
9.5	0.282	23.0	0.289
		49.0	0.299
		88.0	0.175
		138	0.082
		180	0.032
		213	0.018
		258	0.010
		291	0.008

TABLE 6 DISPLACEMENT SHOCK SPECTRUM, SHOT KOA, SURFACE, RADIAL DIRECTION

Station 125.05 Overpressure 84 psi Range 4,200 ft. Gage Number 18 High Frequency		Gage Number 19 High Frequency		Station 125.08 Overpressure 78 psi Range 4,450 ft. Gage Number 7 Low Frequency		Gage Number 1 High Frequency	
f, cps	D, inches	f, cps	D, inches	f, cps	D, inches	f, cps	D, inches
2.5	1.764	3.3	1.089	2.8	1.272	3.2	0.858
9.8	0.292	10.0	0.394	5.6	0.506	9.8	0.127
23.0	0.078	23.0	0.084	9.4	0.248	23.0	0.122
50.0	0.105	49.0	0.125			48.0	0.050
88.0	0.055	90.0	0.065			90.0	0.040
138	0.025	138	0.033			138	0.020
180	0.018	177	0.026			177	0.012
222	0.015	221	0.014			215	0.011
261	0.111	254	0.007			262	0.005
286	0.010	286	0.004			288	—

TABLE 7 DISPLACEMENT SHOCK SPECTRUM, SHOT KOA, SURFACE, RADIAL DIRECTION

Station 125.02 Overpressure 196 psi Range 3,100 ft. Gage Number 17 High Frequency		Station 125.04 Overpressure 88 psi Range 3,940 ft. Gage Number 5 Low Frequency		Gage Number 5 High Frequency		Station 125.05 Overpressure 84 psi Range 4,200 ft. Gage Number 6 Low Frequency		Gage Number 3 Low Frequency	
f, cps	D, inches	f, cps	D, inches	f, cps	D, inches	f, cps	D, inches	f, cps	D, inches
2.9	—	2.7	0.657	2.8	—	2.6	1.156	2.8	0.508
10.1	—	5.4	0.151	10.0	0.347	5.1	0.850	6.2	0.254
23.0	0.245	8.5	0.124	23.0	0.235	8.5	0.419	8.9	0.106
51.0	0.146			50.0	0.112				
88.0	0.184			90.0	0.062				
138	0.084			138	0.036				
181	0.040			180	0.026				
220	0.028			221	0.012				
260	0.014			282	0.007				
286	0.011			288	0.003				

TABLE 8 DISPLACEMENT SHOCK SPECTRUM, SHOT KOA, INSIDE SHELTER, VERTICAL DIRECTION

Station 125.01 Overpressure 196 psi Range 3,200 ft Gage Number 20 High Frequency		Station 125.03* Overpressure 86 psi Range 3,940 ft Gage Number 6 High Frequency	
f, cps	D, inches	f, cps	D, inches
3.0	—	3.0	3.444
10.1	1.517	9.9	1.468
23	0.627	23	0.280
49	0.111	51	0.045
90	0.032	91	0.016
138	0.023	137	0.004
181	0.015	179	0.004
221	0.020	222	—
254	0.017	262	0.002
283	0.013	286	0.002

* Low-frequency Gage Number 2 records at this station were not recoverable.

TABLE 9 DISPLACEMENT SHOCK SPECTRUM, SHOT KOA, INSIDE SHELTER, RADIAL DIRECTION

Station 125.01 Overpressure 196 psi Range 3,200 ft Gage Number 11 High Frequency		Station 125.03* Overpressure 86 psi Range 3,940 ft Gage Number 8 High Frequency	
f, cps	D, inches	f, cps	D, inches
3.0	4.129	3.1	—
9.9	1.187	10.1	—
23	0.724	23	0.173
48	0.152	49	0.020
89	0.041	91	0.013
138	0.020	137	0.008
180	0.016	178	0.004
219	0.008	221	0.002
250	0.003	254	0.001
288	0.003	288	0

* Low-frequency Gage Number 10 records at this station were not recoverable.

percent) than the vertical components (Gage 3) for all frequencies except between 10 and 100 cps when the peaking occurs in the vertical component (Figures 20 and 19).

At 90 psi (Station 125.09) the radial components (Gage 13) are less than the vertical (Gage 22) except at the high-frequency range (greater than 200 cps) as shown in Figures 22 and 21.

The vertical displacements inside the shelter at 90 psi (Gage 7, Station 125.10) do not show the peaking at 40 cps that the outside (Gage 22, Station 125.09) measurements do. The displacements are nearly the same as for outside up to 10 cps but are attenuated (factor of 7) in the intermediate-frequency range (20 to 100 cps) from the values measured in the free field adjacent to the structure (Figures 23 and 21).

The radial displacements inside the shelter (Gage 9, Station 125.10) and outside (Gage 13, Station 125.09) at 90 psi are similar up to 10 cps. Displacements inside show high attenuation (85 percent) at high frequency (greater than 100 cps) as compared with displacements outside (Figures 24 and 22).

Shot Koa. At Station 125.05, the adjacent gages (14 and 23) give nearly duplicate records for the vertical displacements at 84 psi (Figures 31 and 32).

The vertical displacements measured by the low-frequency gages (L1 and L4, Stations 125.04 and 125.06) for 86 and 78 psi agree fairly well up to 6 cps. Because these gages were designed for much greater displacements than those measured, their accuracy is in doubt (Figures 27 and 38).

The radial displacements measured by the low-frequency gages (L5, L3, L6, and L7, Stations 125.04, 125.05, and 125.06) for 86, 84, and 78 psi show considerable scatter. Records are not considered satisfactory (Figures 30, 33, 34, and 40).

The vertical displacements measured by the low-frequency gage (L1, Station 125.04) at 86 psi are consistent with low-frequency components measured by the gage (23, Station 125.05) at 84 psi (Figures 27 and 32).

The radial displacements for adjacent gages (16 and 19, Station 125.05) agree closely (within 20 percent) and indicate a dip in the spectrum (half of normal trend) at about 20 cps (Figures 35 and 36).

At Station 125.05, the vertical displacement (Gage 23) for 84 psi is generally higher than the radial displacement (Gage 19) for the entire frequency range, being from about three times as great at 3 cps to slightly greater at high frequency (above 100 cps); but with the largest difference (six times) at 20 cps, where the peak in the vertical displacements corresponds to the dip in the radial displacements (Figures 32 and 36).

The vertical displacements inside the shelter (Gage 20, Station 125.01) are considerably attenuated (factor of 8) in the intermediate-frequency range (50 to 200 cps) from the values measured in the free field (Gage 10, Station 125.02) adjacent to the structure (Figures 41 and 25).

The radial displacements inside the shelter (Gage 11, Station 125.01) are lower (factor of 4) over the entire frequency range from the values measured in the free field (Gages 17 and L5, Stations 125.02 and 125.04) adjacent to the structure (Figures 42, 26, and 30).

The vertical displacements inside the shelter (Gage 6, Station 125.03) are higher (average factor of 3) in the low-frequency range (3 to 20 cps), equal at 20 cps, then extremely attenuated (factor of 10 to 20) in the frequency range of 20 to 300 cps from the values measured in the free field (Gage 2, Station 125.06) adjacent to the structure (Figures 43 and 37).

The radial displacements inside the shelter (Gage 8, Station 125.03) are equal at a frequency of 20 cps and then gradually attenuated (factor of 7) over the range of 20 to 300 cps from the values measured in the free field (Gage 1, Station 125.06) adjacent to the structure (Figures 44 and 39).

Shot Cactus and Operation Plumbbob. At 110 psi, the vertical displacements of Shot Cactus (Gage 3, Station 125.08) are significantly less (one third to one fifth) than for the shots during Operation Plumbbob up to about 20 cps where they are almost equal. Above 50 cps, the vertical displacements for Shot Cactus are two to four times greater than for the Plumbbob shots (Figures 19 and 2).

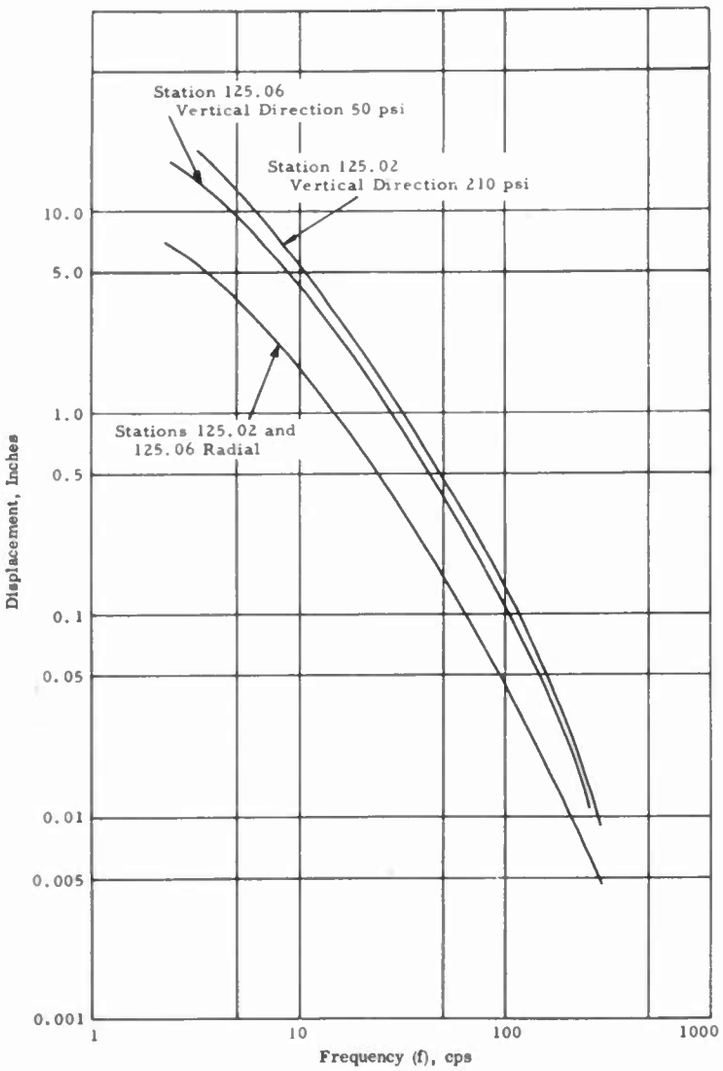

Figure 15 Displacement shock spectrum, predicted Koa event.

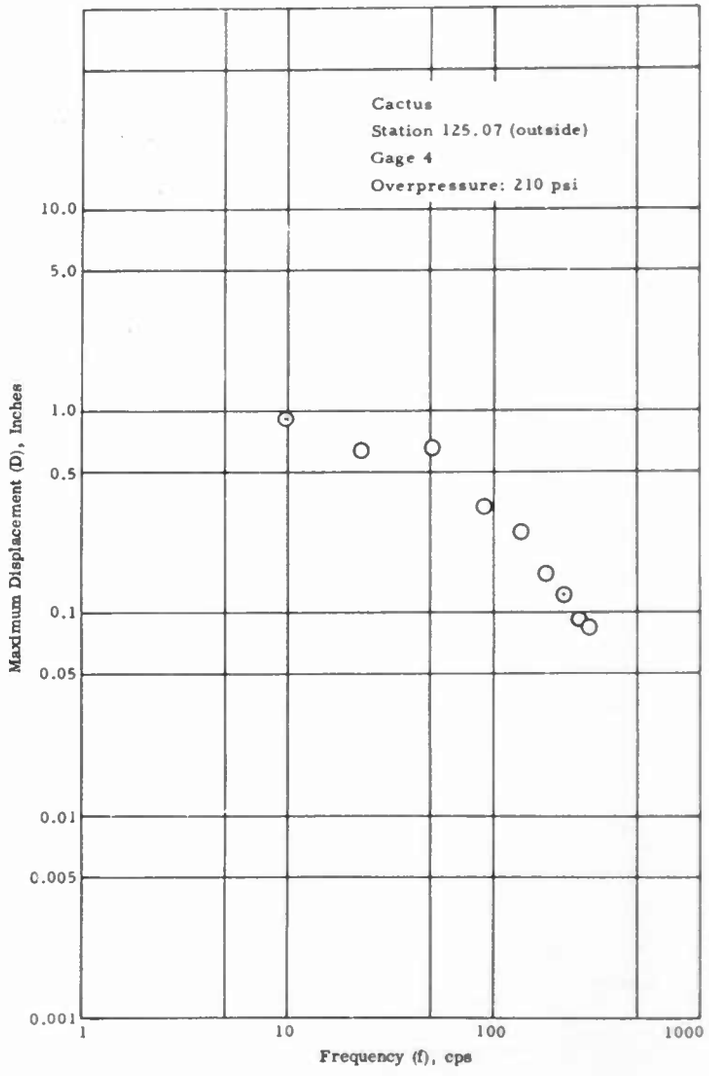

Figure 16 Displacement shock spectrum, vertical direction, Gage 4.

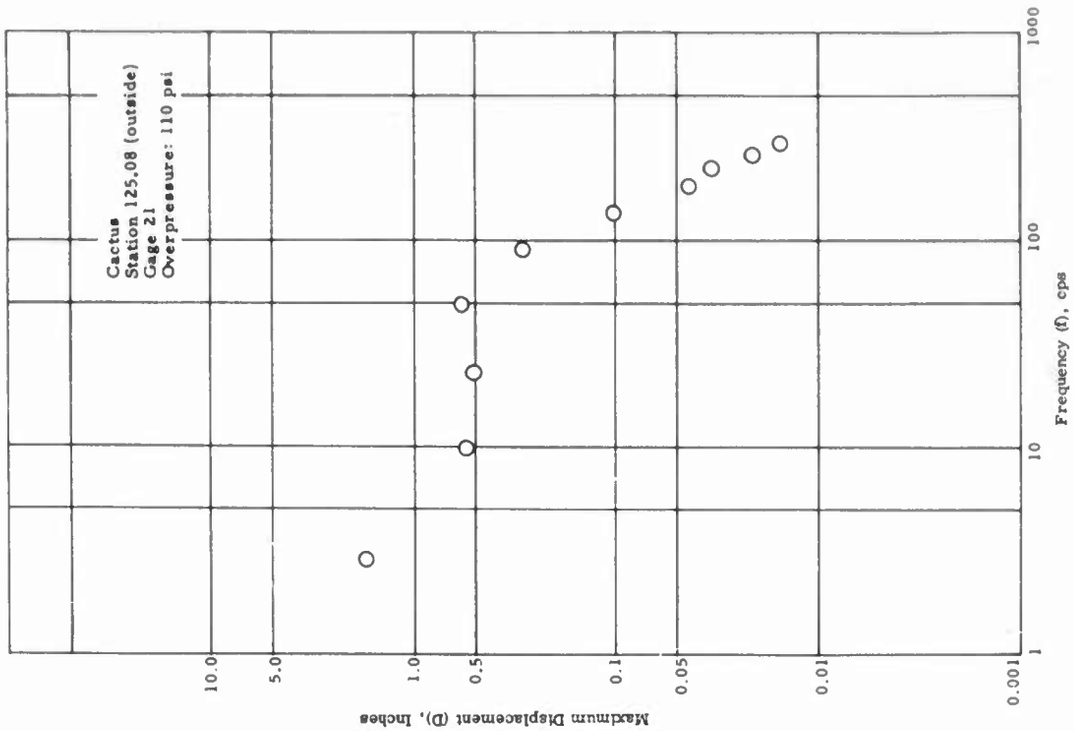

Figure 18 Displacement shock spectrum, vertical direction, Gage 21.

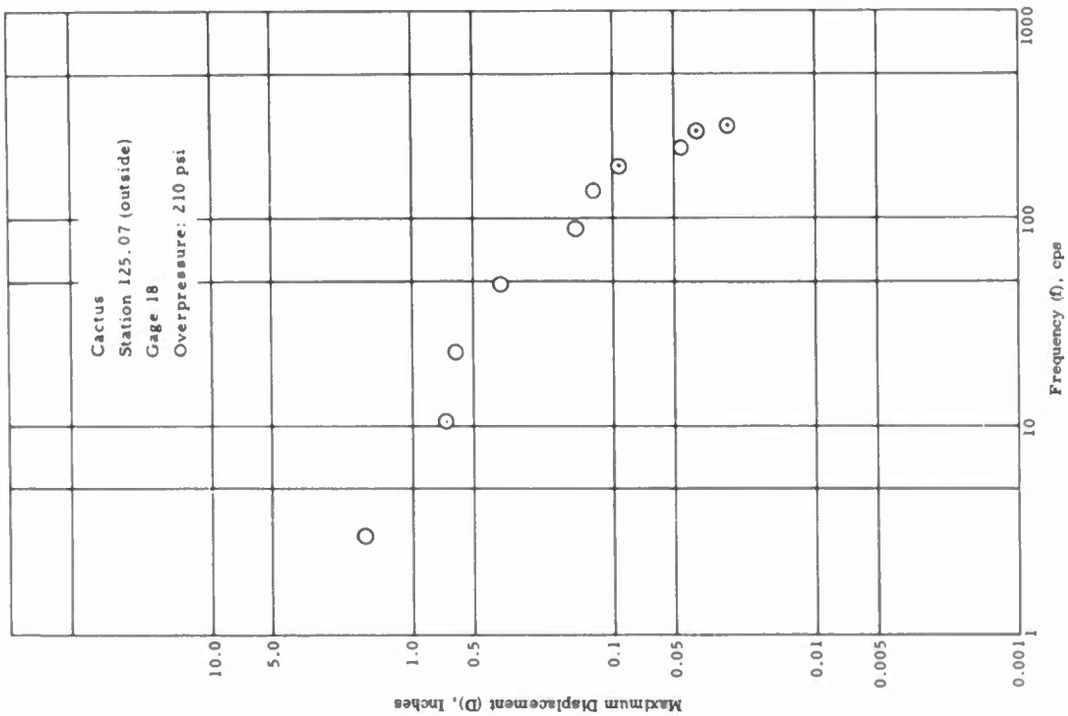

Figure 17 Displacement shock spectrum, radial direction, Gage 18.

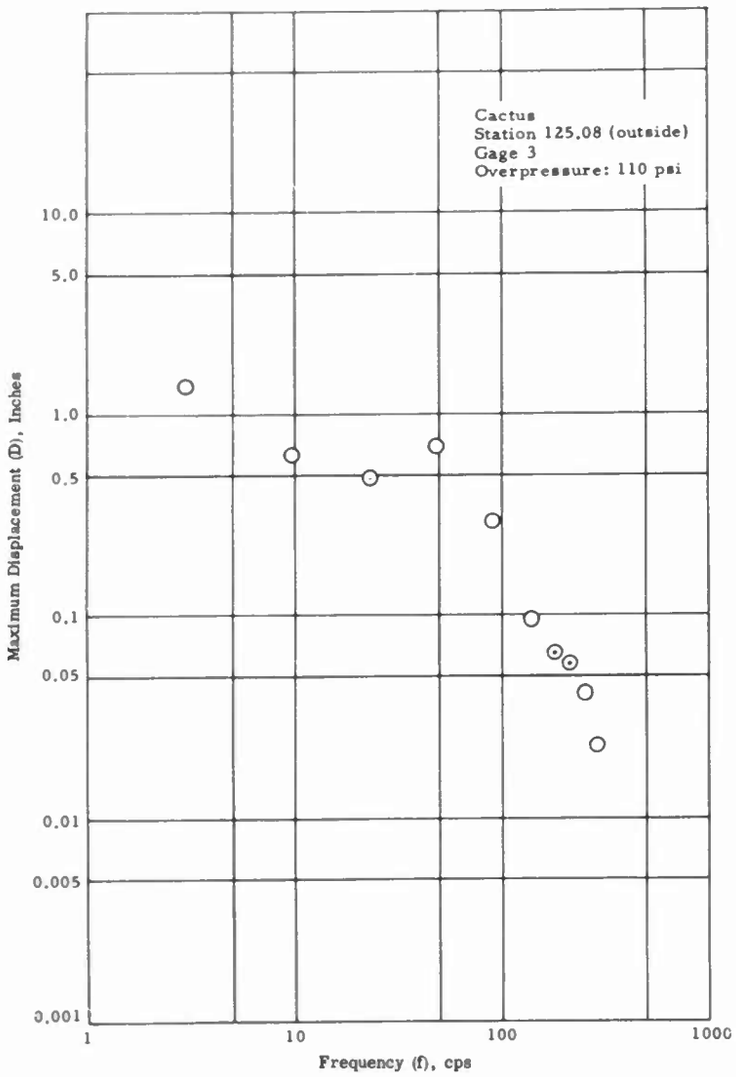

Figure 19 Displacement shock spectrum, vertical direction, Gage 3.

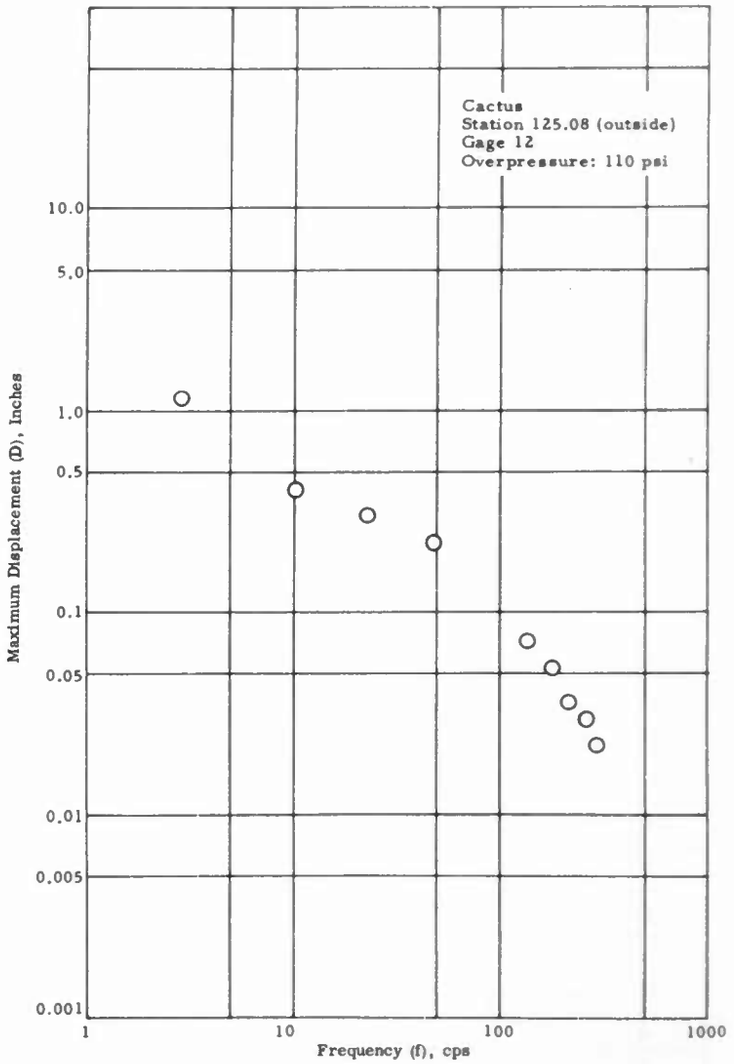

Figure 20 Displacement shock spectrum, radial direction, Gage 12.

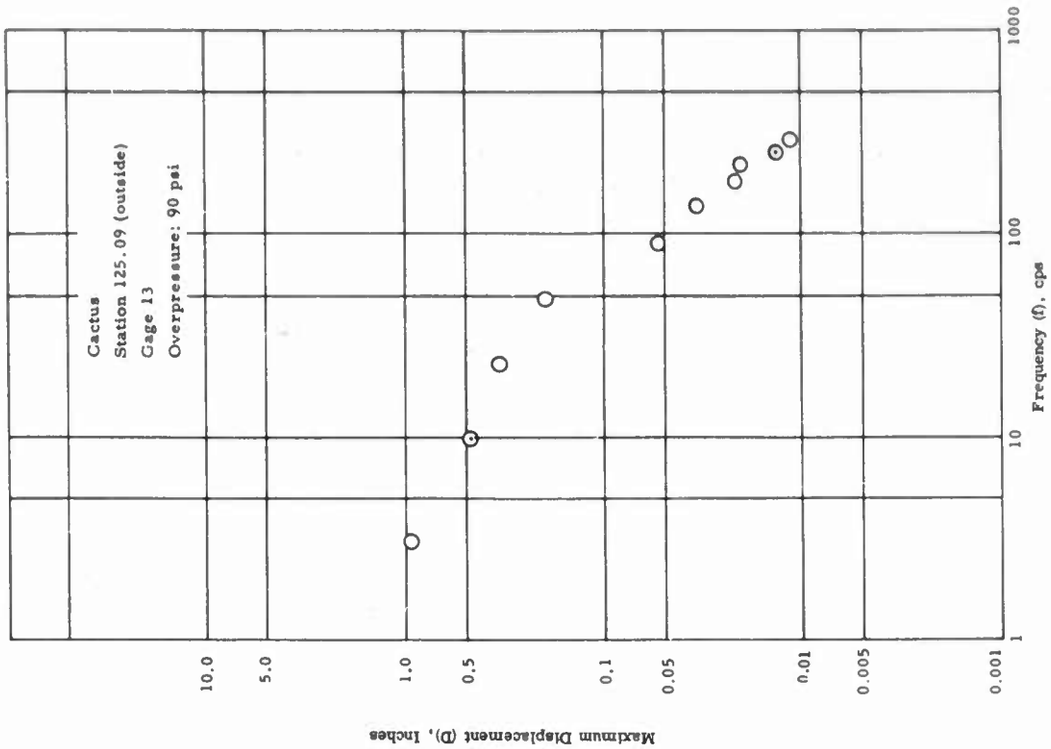

Figure 22 Displacement shock spectrum, radial direction, Gage 13.

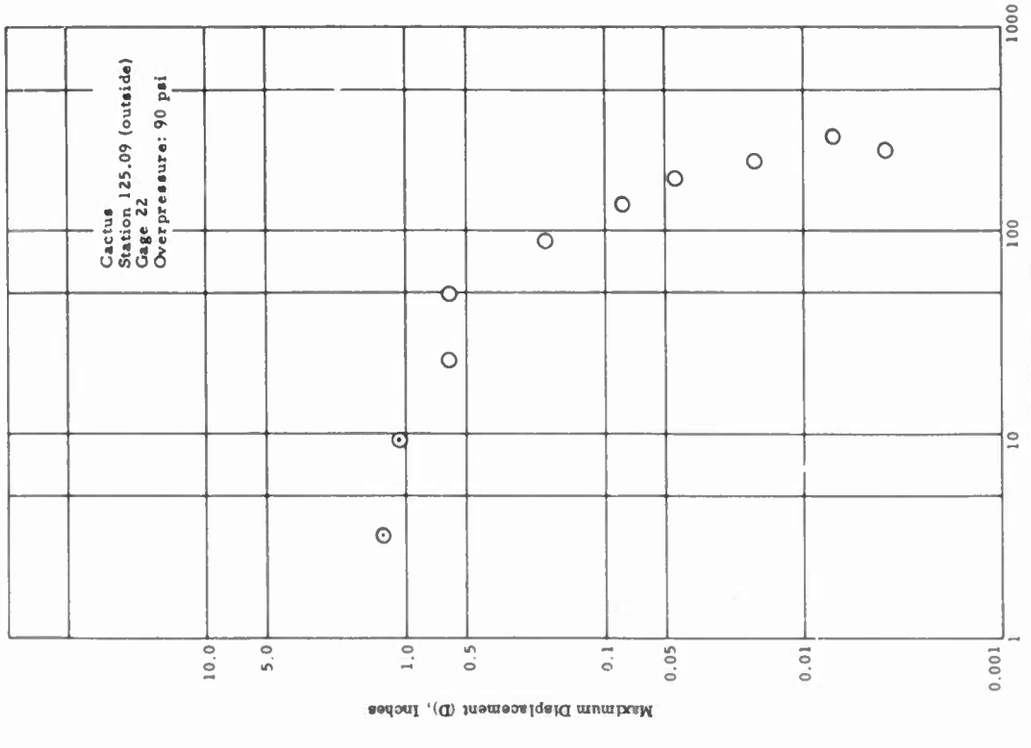

Figure 21 Displacement shock spectrum, vertical direction, Gage 22.

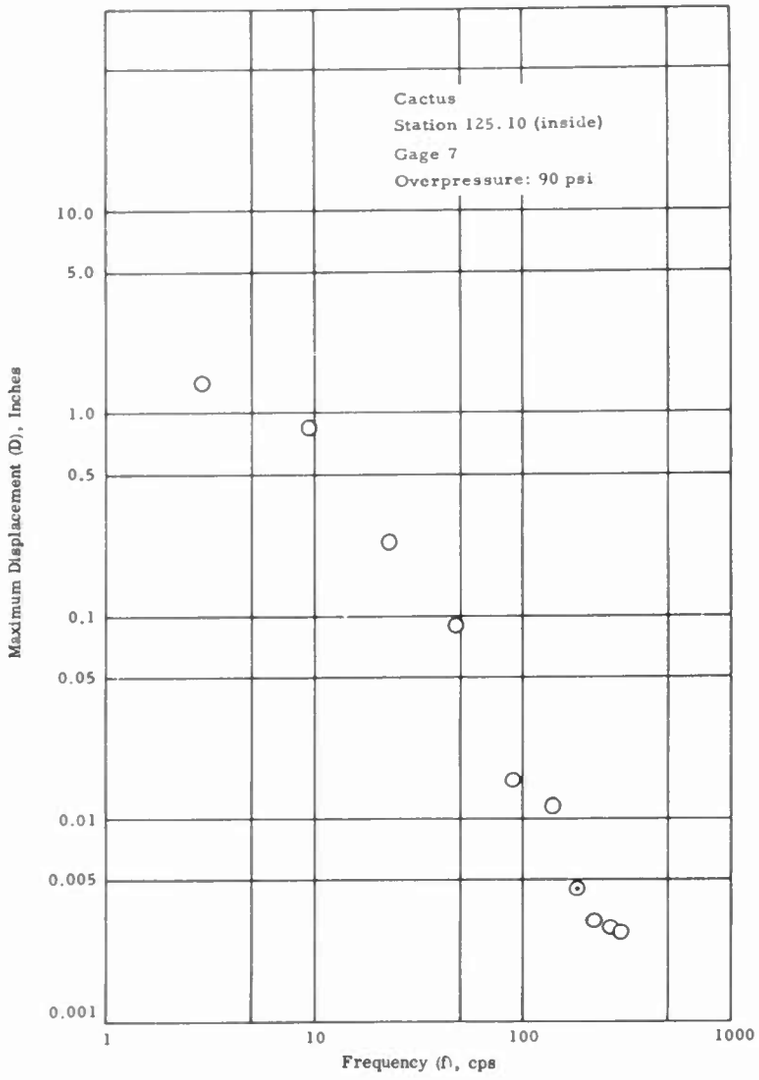

Figure 23 Displacement shock spectrum, vertical direction, Gage 7.

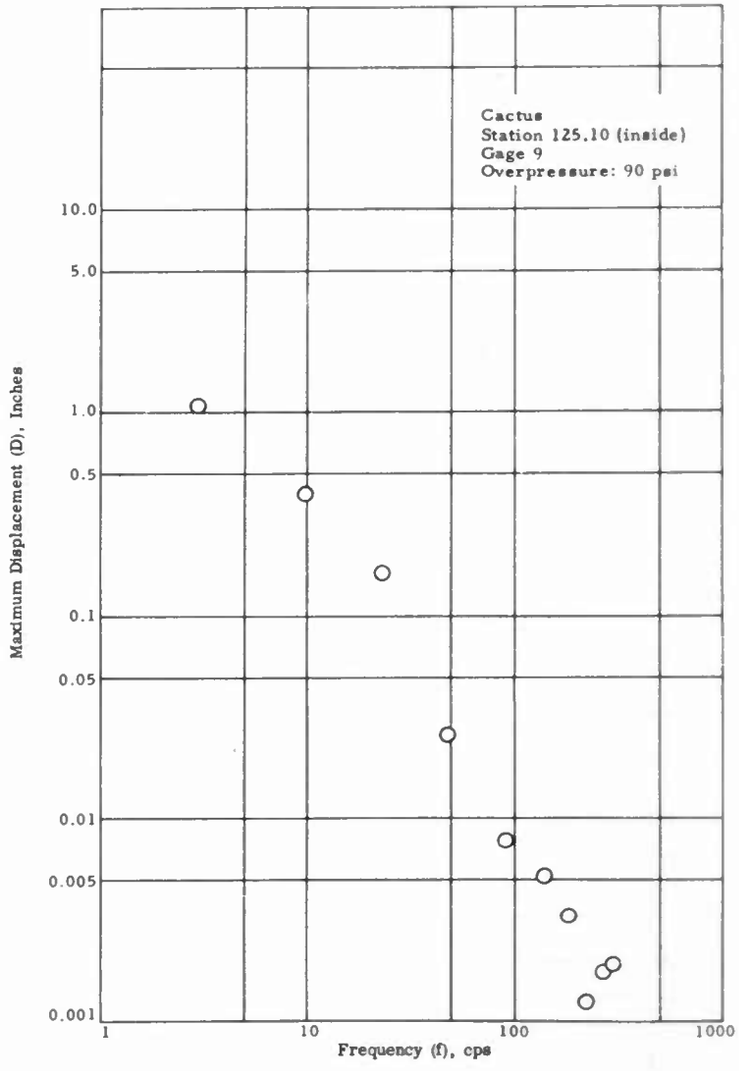

Figure 24 Displacement shock spectrum, radial direction, Gage 9.

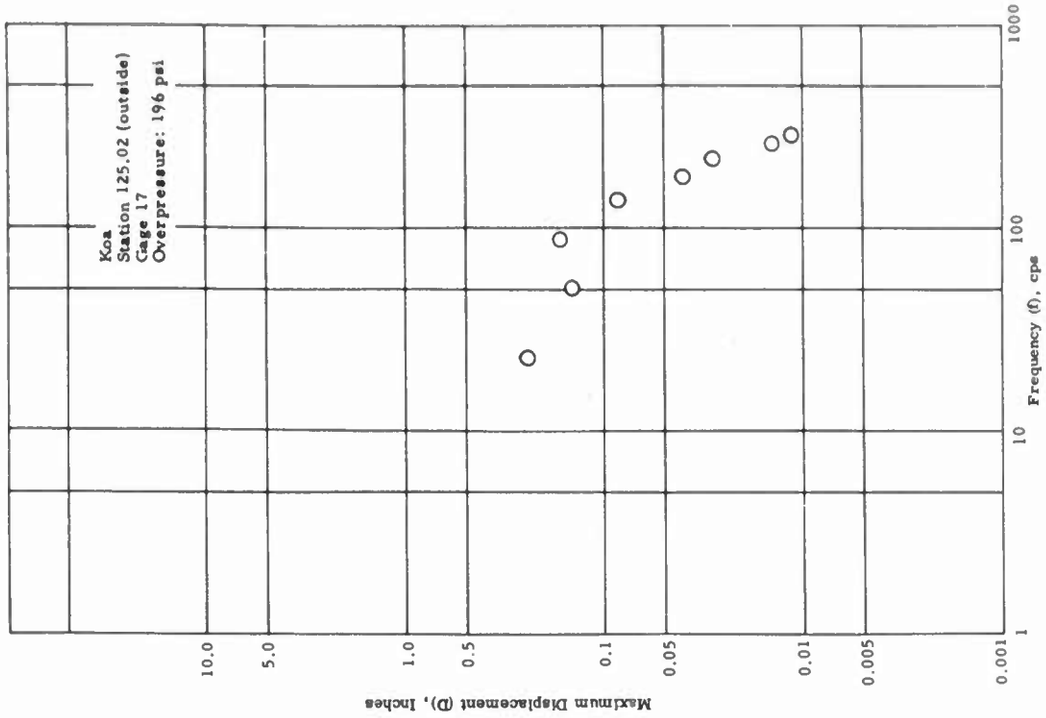

Figure 26 Displacement shock spectrum, radial direction, Gage 17.

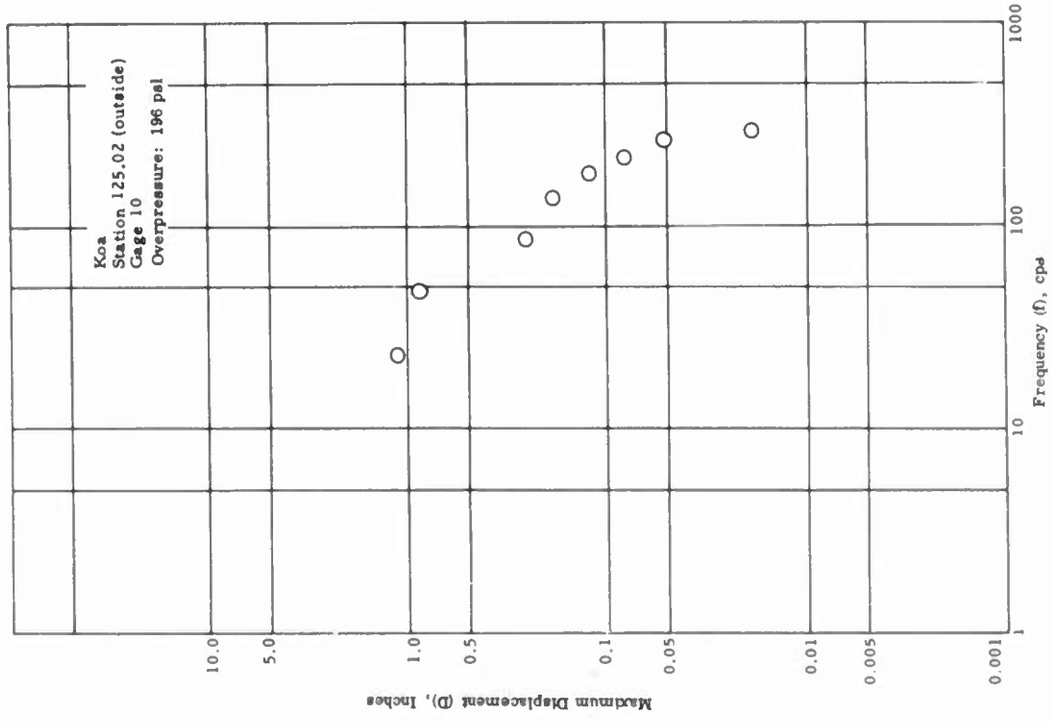

Figure 25 Displacement shock spectrum, vertical direction, Gage 10.

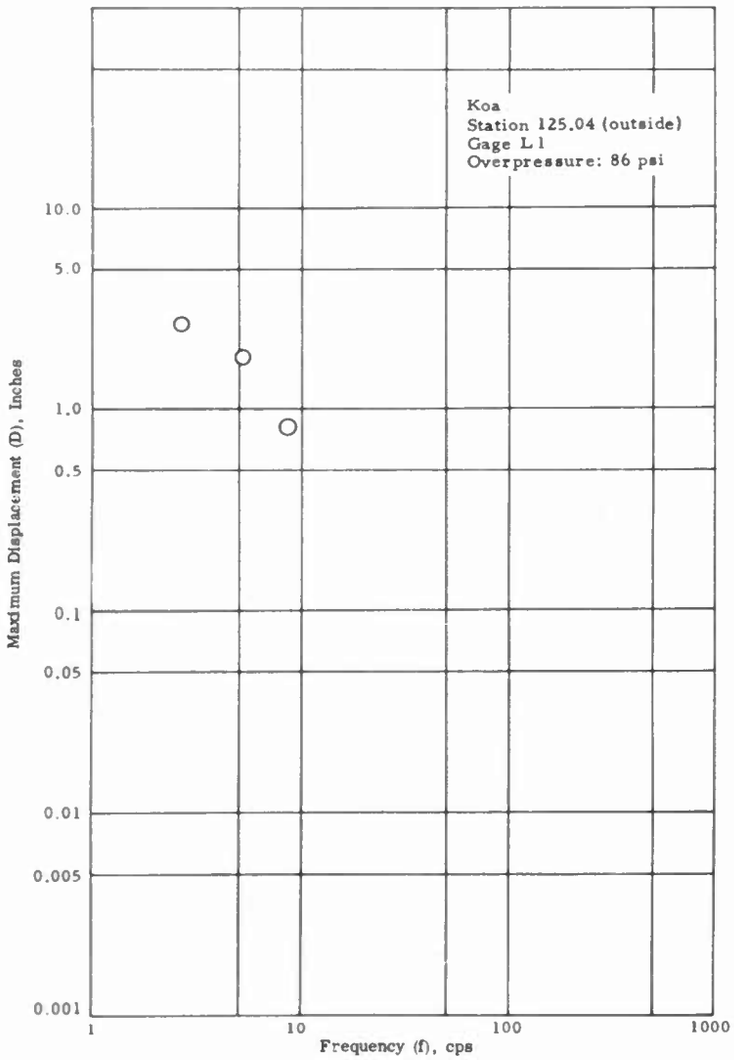

Figure 27 Displacement shock spectrum, vertical direction, Gage L1.

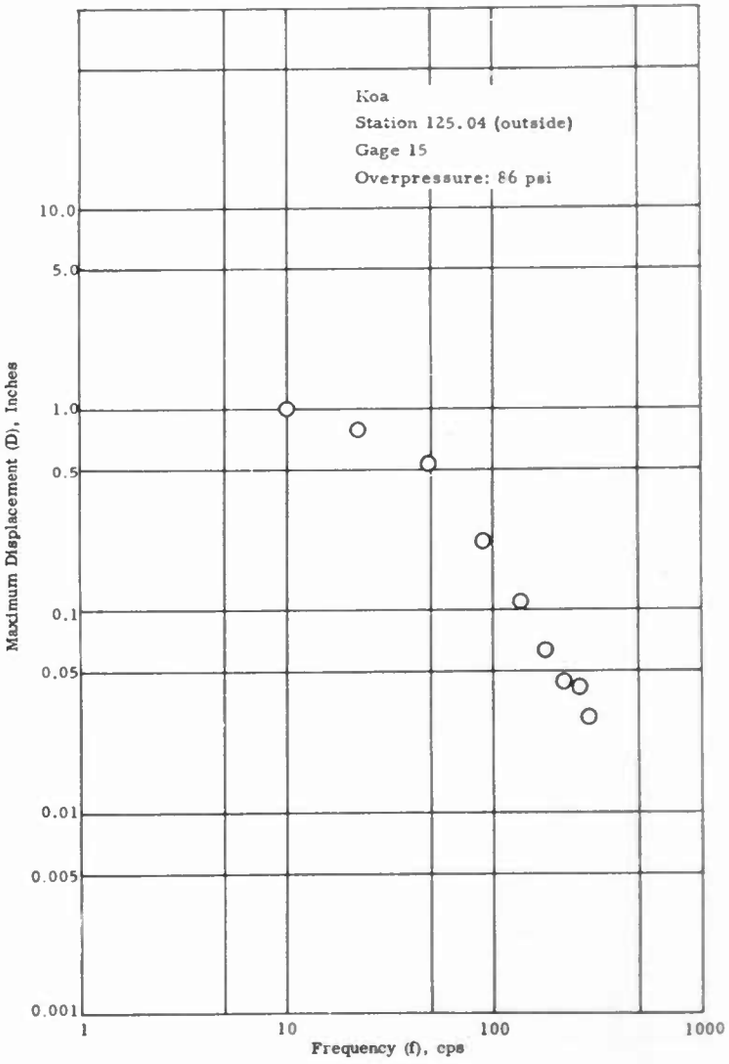

Figure 28 Displacement shock spectrum, vertical direction, Gage 15.

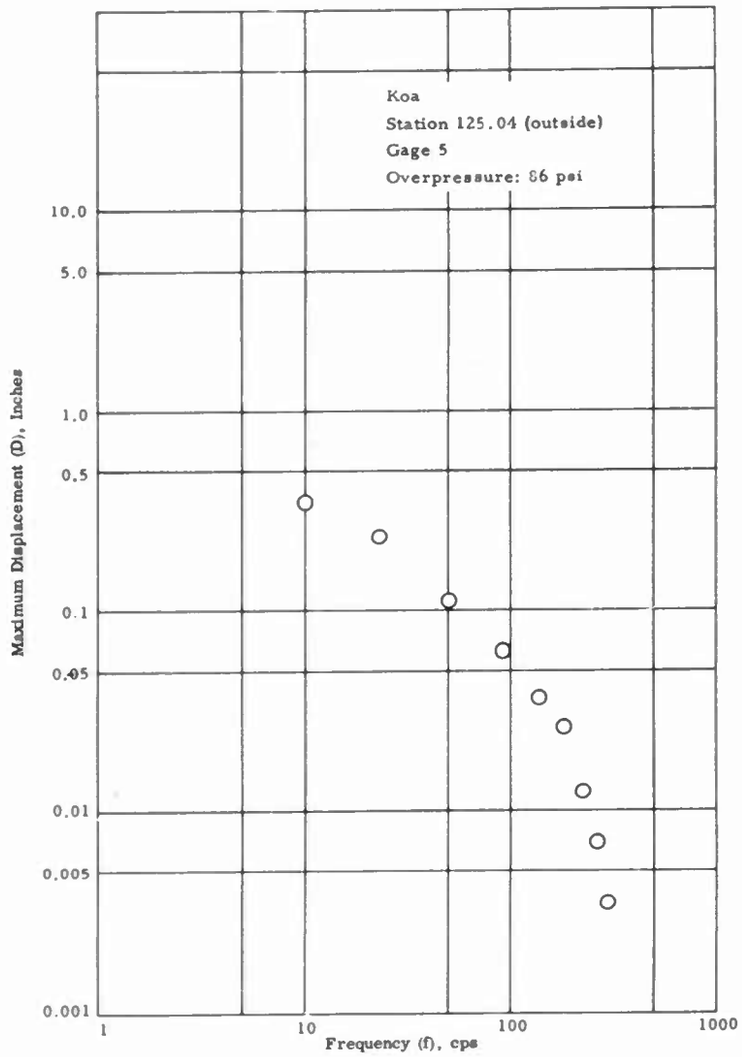

Figure 29 Displacement shock spectrum, radial direction, Gage 5.

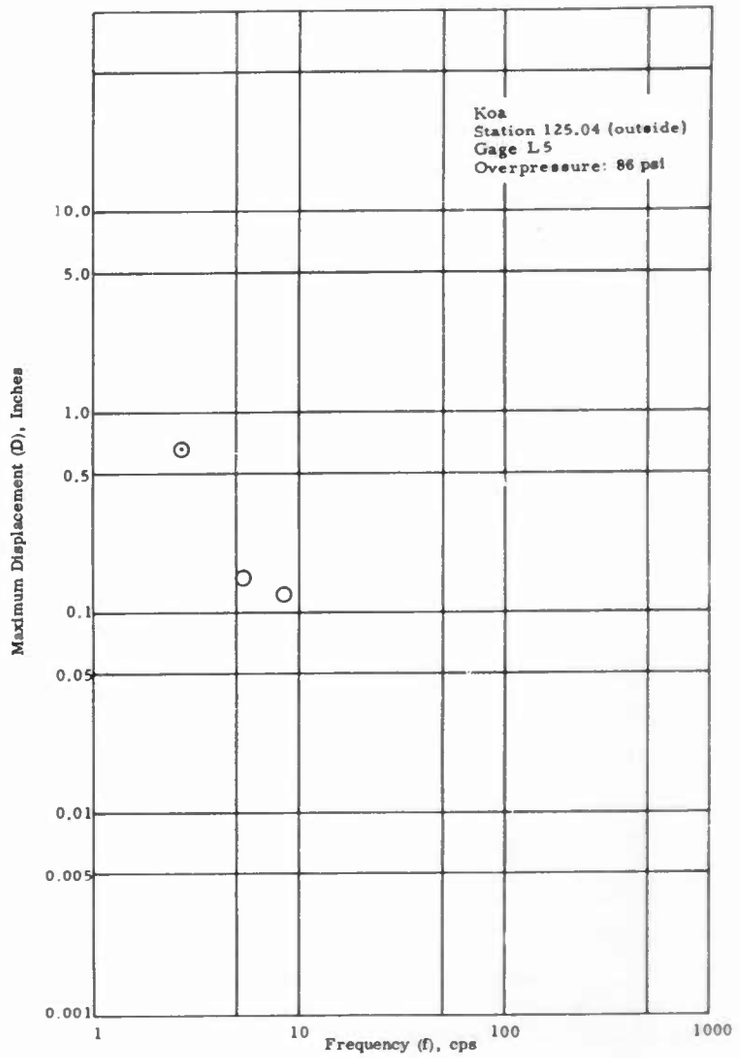

Figure 30 Displacement shock spectrum, radial direction, Gage L5.

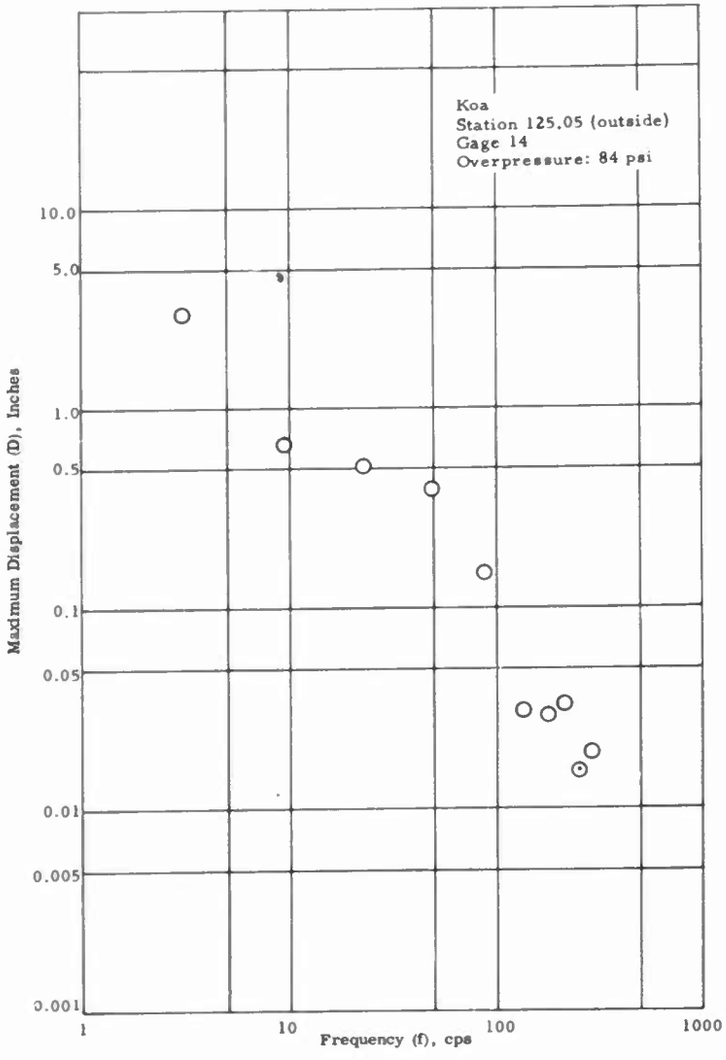

Figure 31 Displacement shock spectrum, vertical direction, Gage 14.

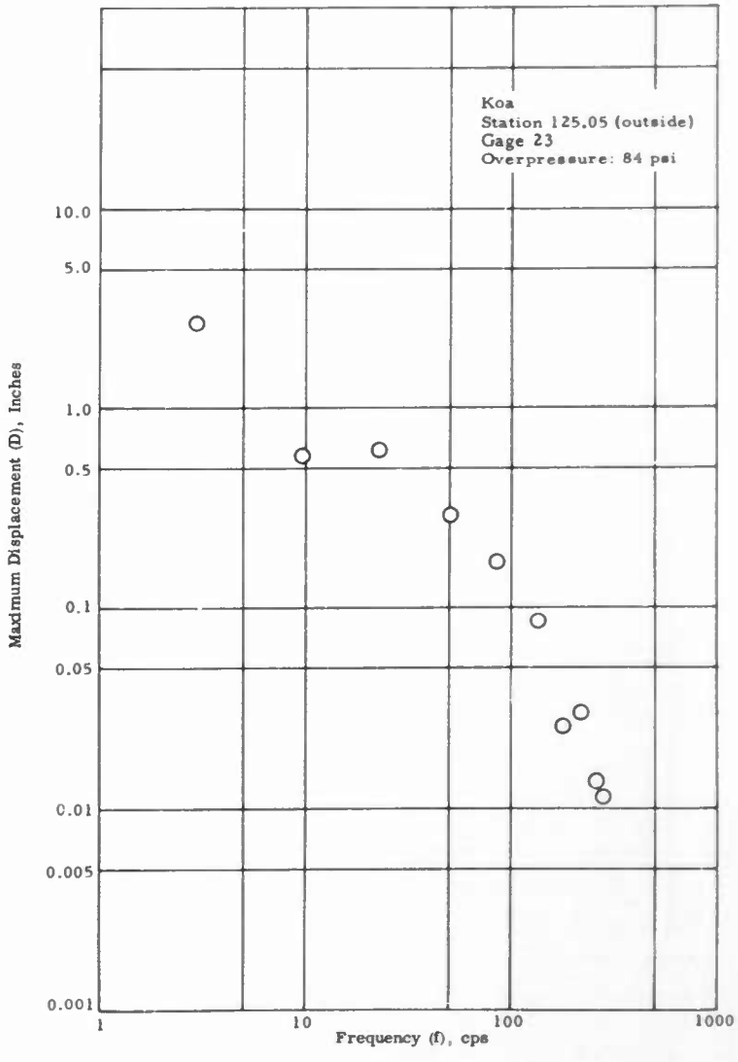

Figure 32 Displacement shock spectrum, vertical direction, Gage 23.

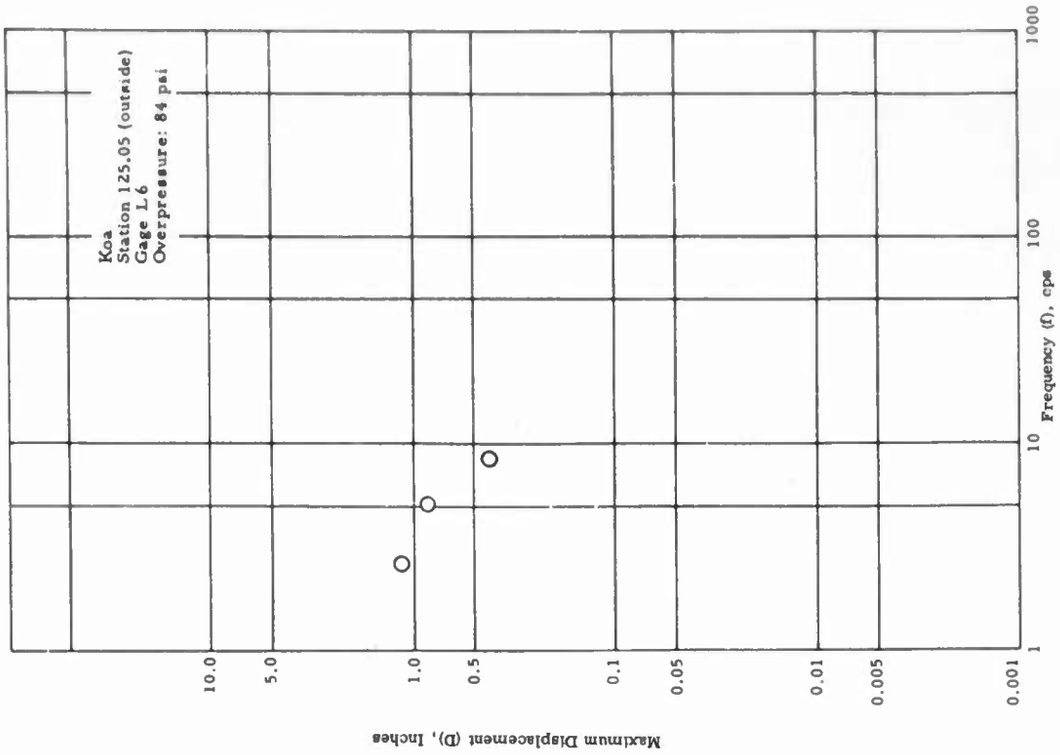

Figure 34 Displacement shock spectrum, radial direction, Gage L6.

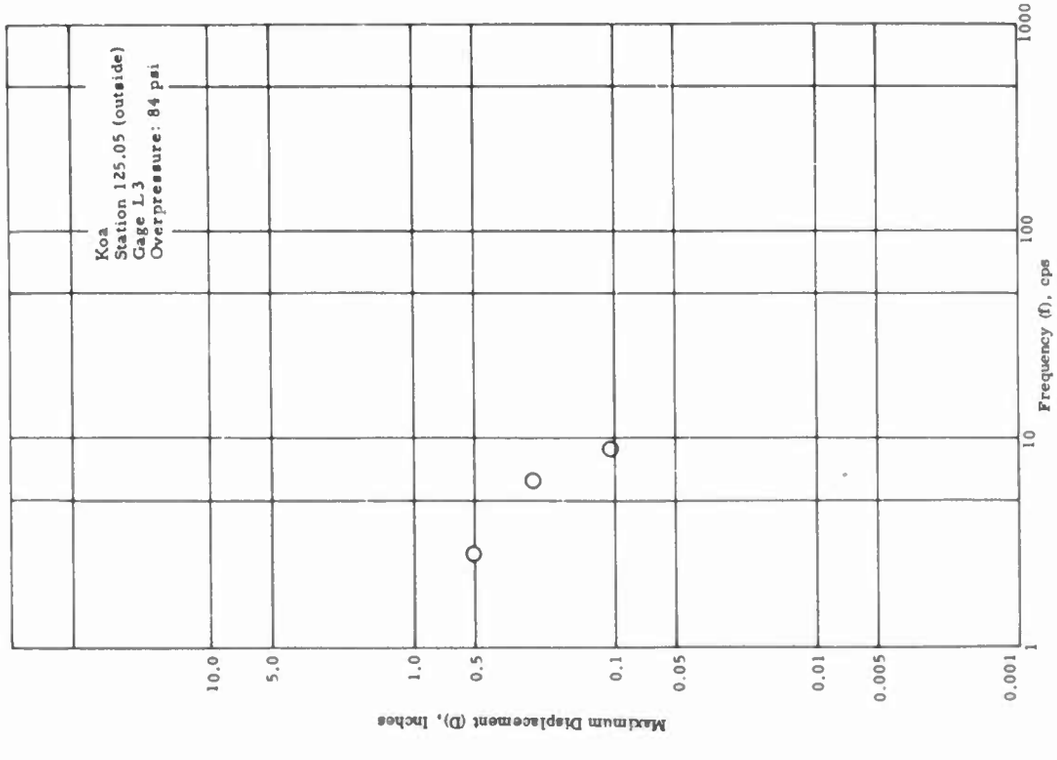

Figure 33 Displacement shock spectrum, radial direction, Gage L3.

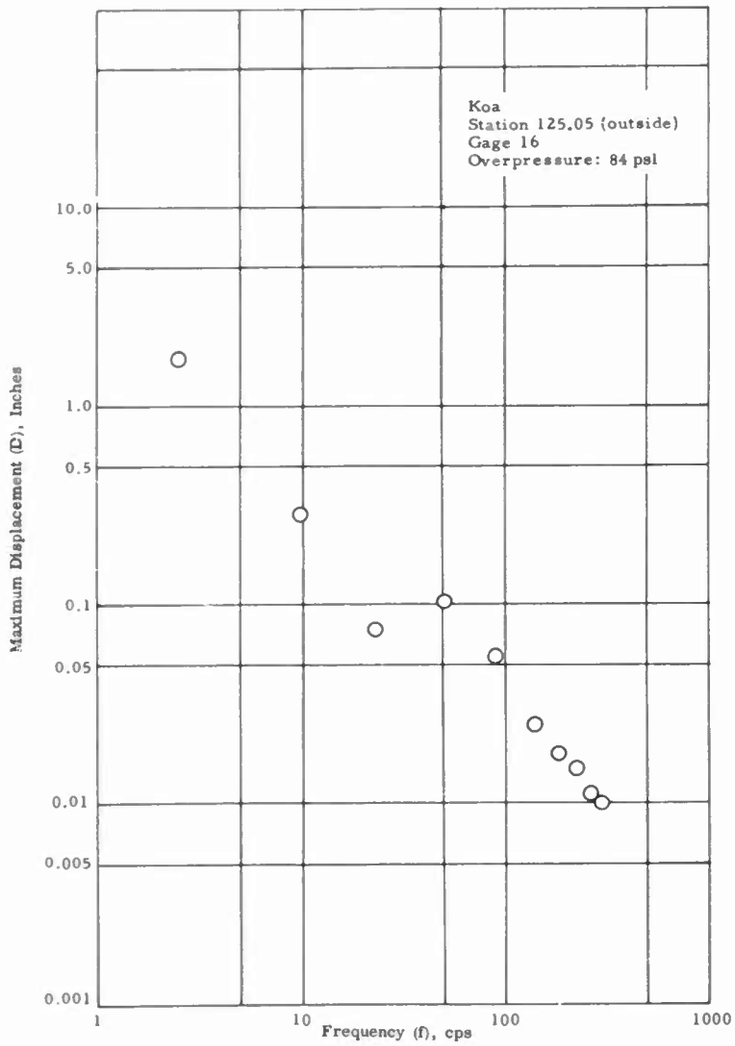

Figure 35 Displacement shock spectrum, radial direction, Gage 16

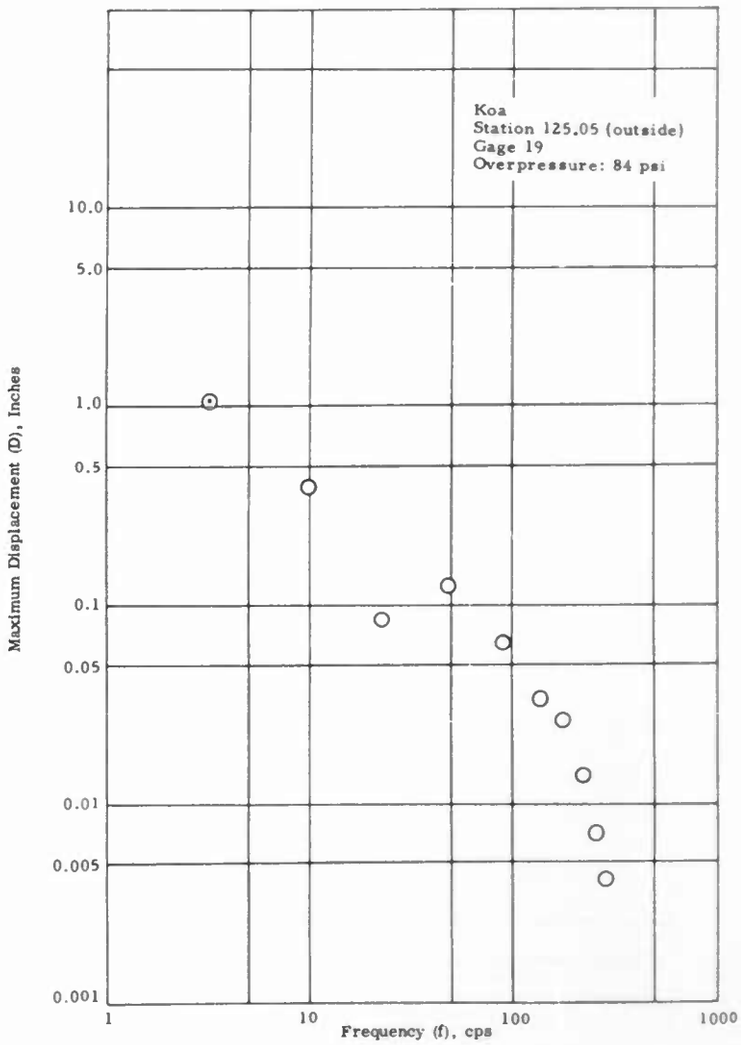

Figure 36 Displacement shock spectrum, radial direction, Gage 19

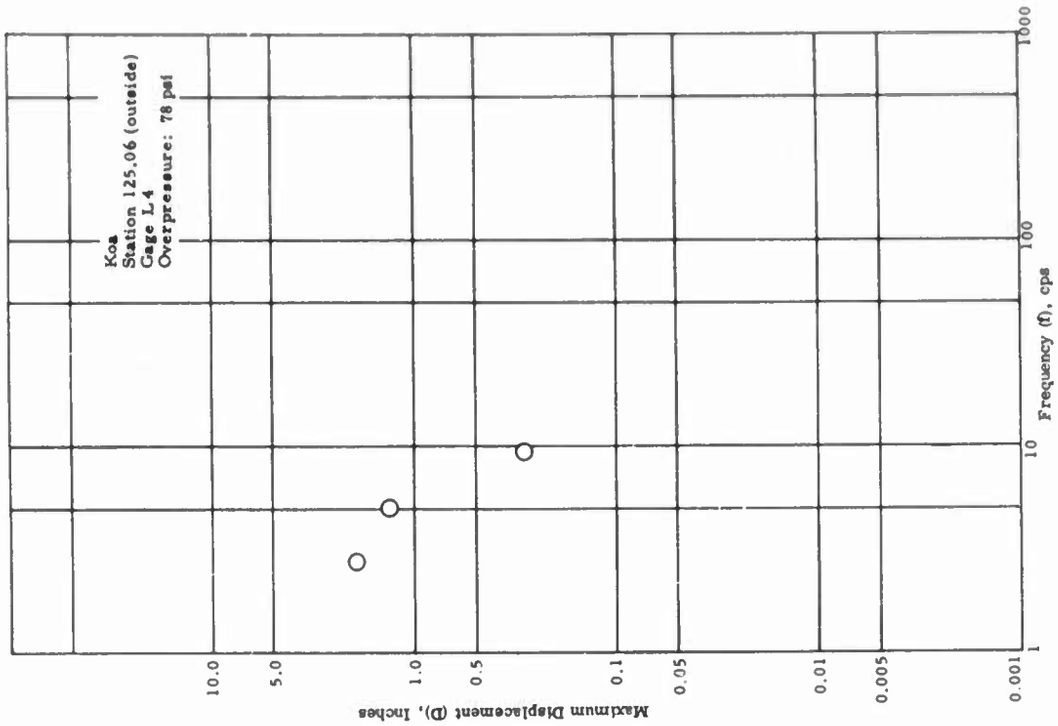

Figure 38 Displacement shock spectrum, vertical direction, Gage L4.

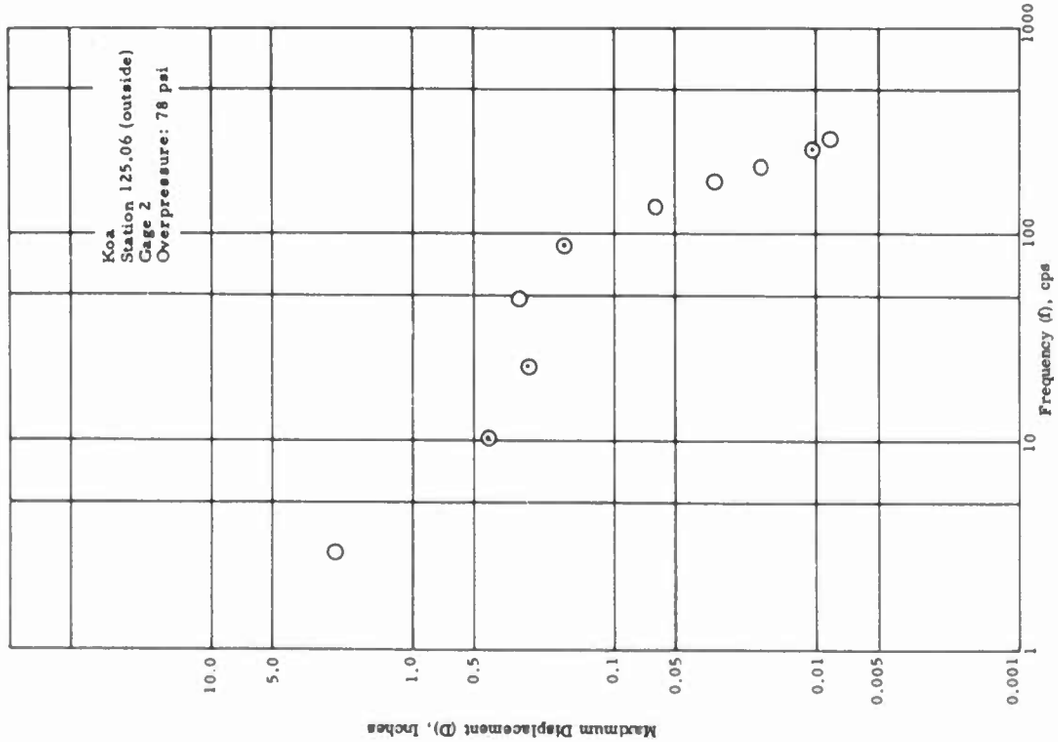

Figure 37 Displacement shock spectrum, vertical direction, Gage 2.

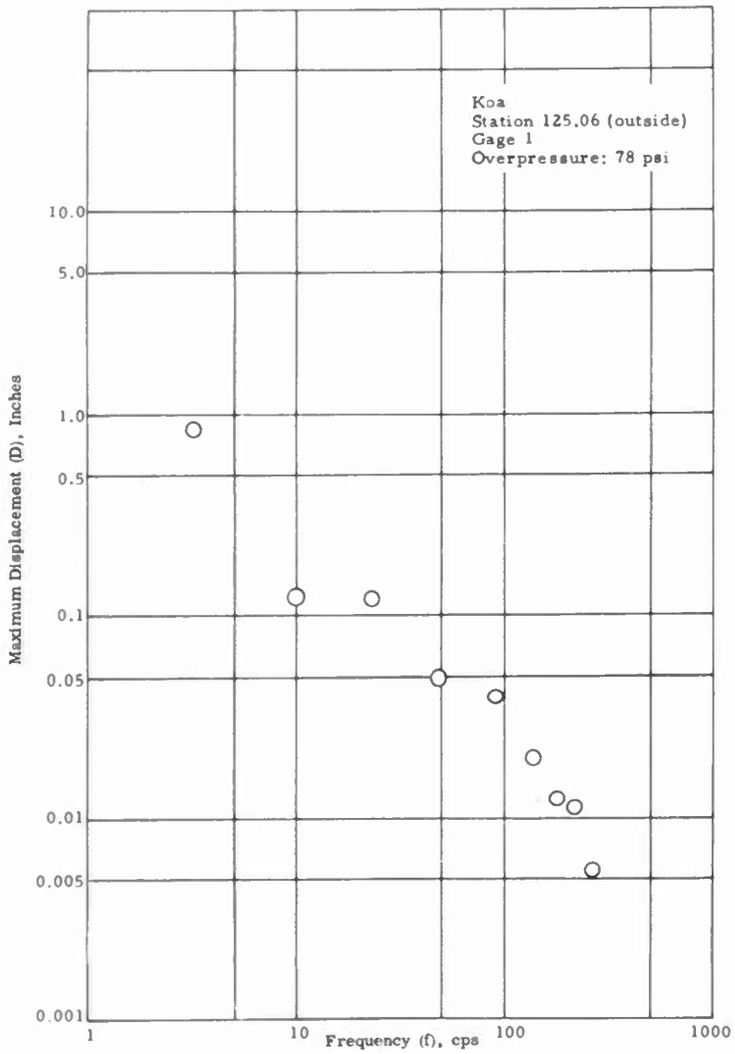

Figure 39 Displacement shock spectrum, radial direction, Gage 1.

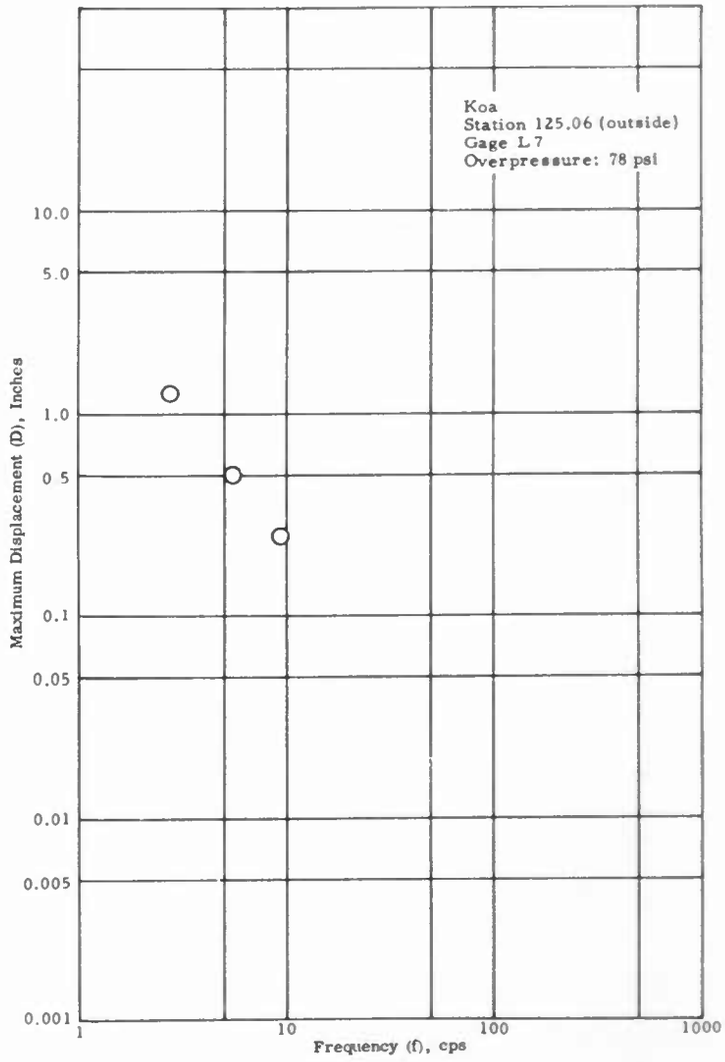

Figure 40 Displacement shock spectrum, radial direction, Gage L7.

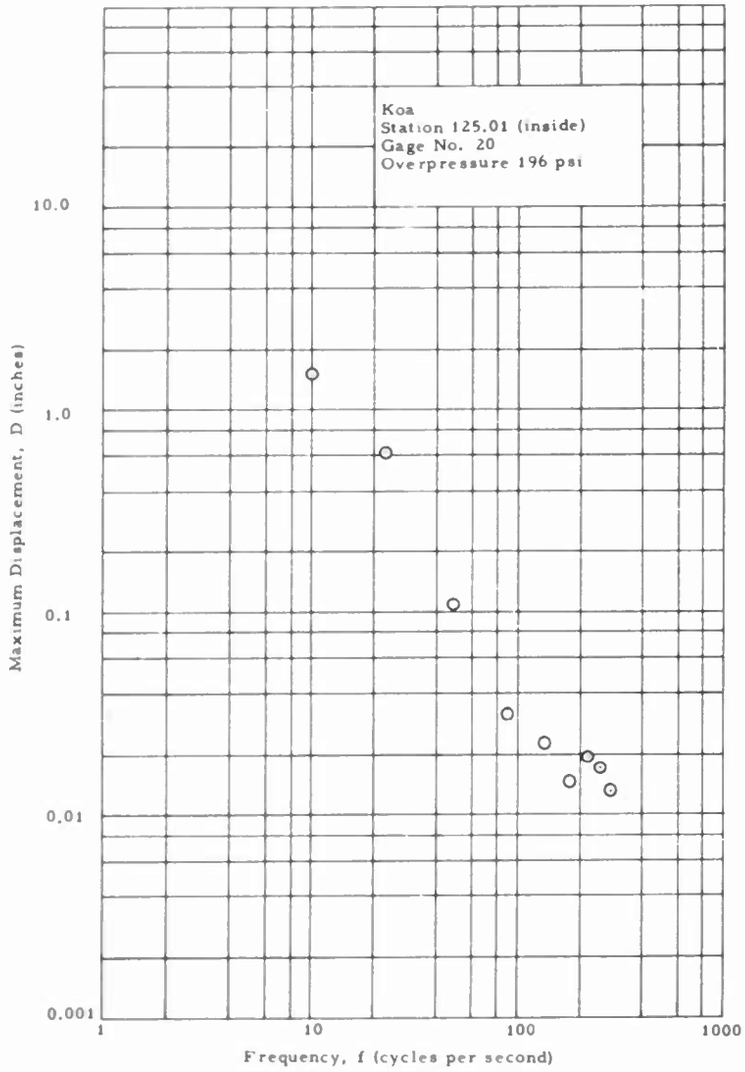

Figure 41 Displacement shock spectrum, vertical direction, Gage 20.

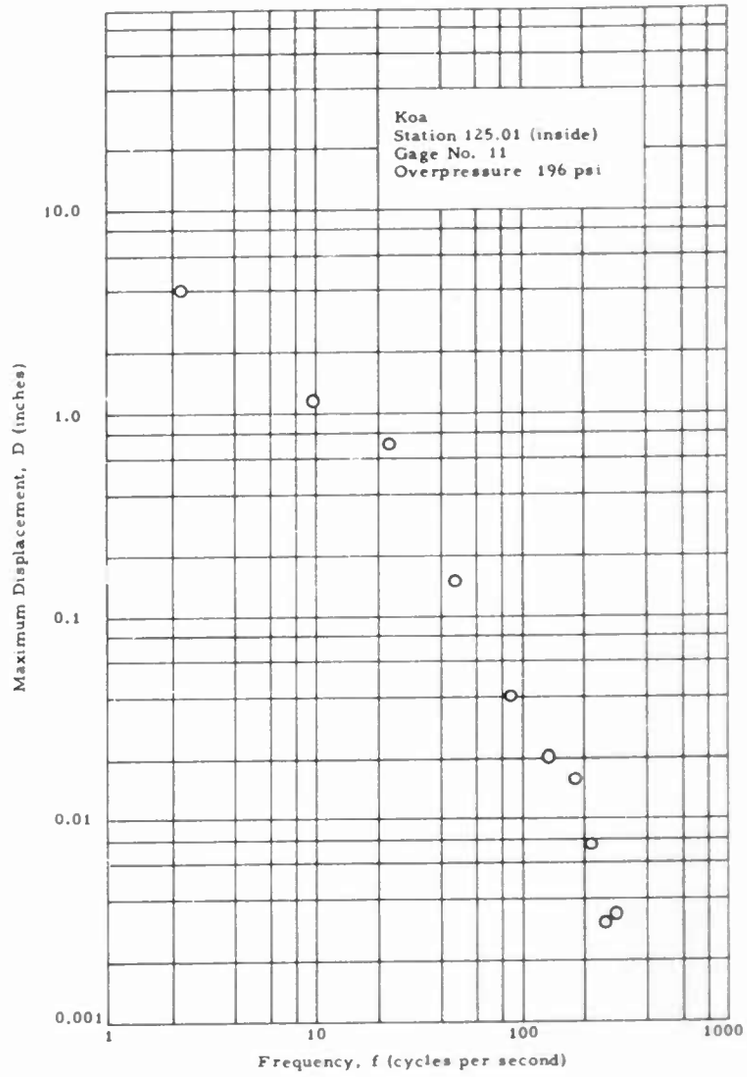

Figure 42 Displacement shock spectrum, radial direction, Gage 11.

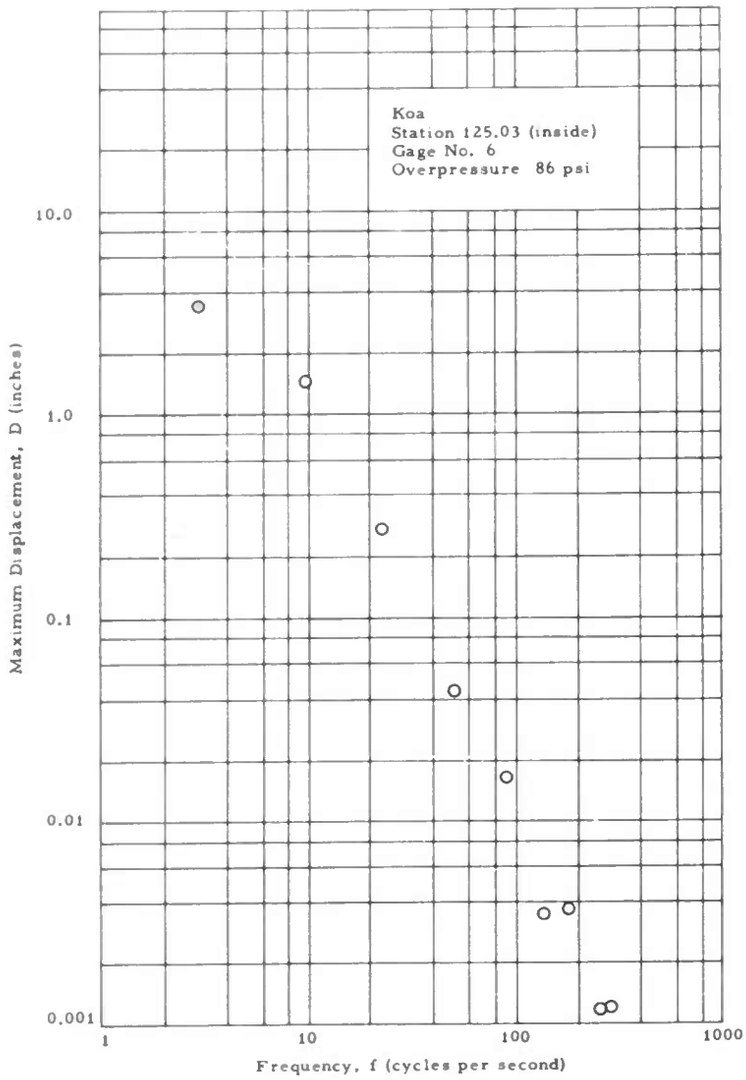

Figure 43 Displacement shock spectrum, vertical direction, Gage 6.

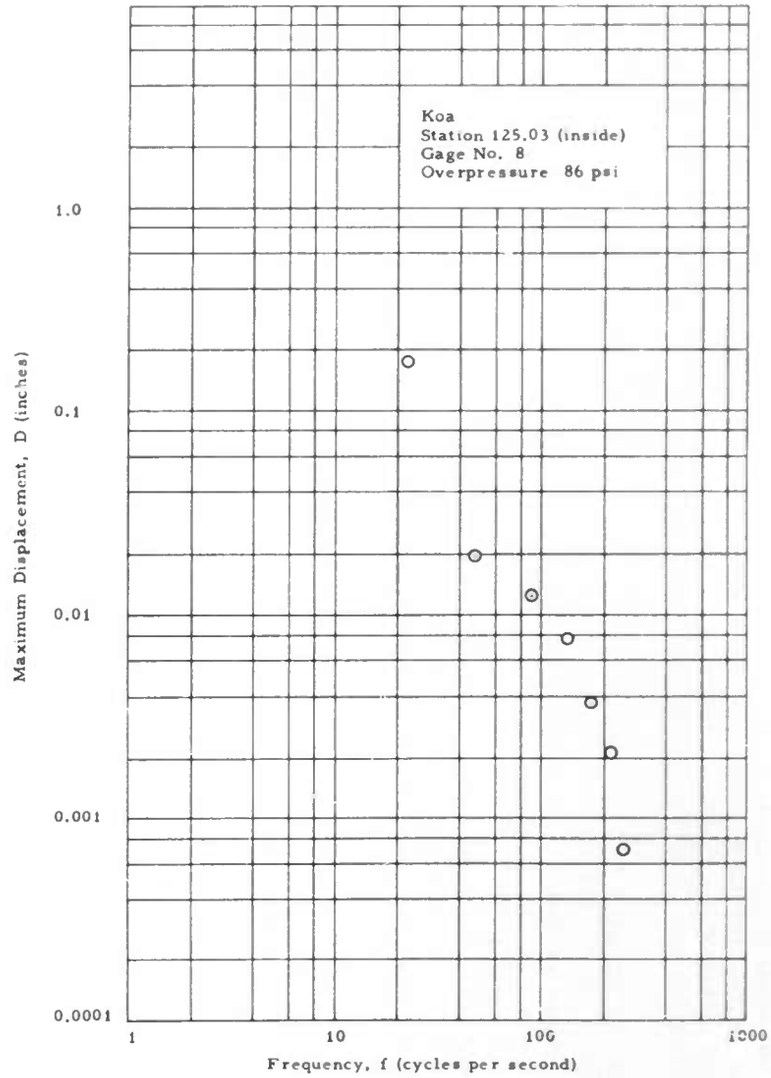

Figure 44 Displacement shock spectrum, radial direction, Gage 8.

The radial displacements at 110 psi for Shot Cactus (Gage 12, Station 125.08) are about the same as those for the Plumbbob shots up to 10 cps. For the higher frequencies, the displacements for Shot Cactus are two to four times greater than those for the Plumbbob shots (Figures 20 and 3).

Shots Cactus and Koa. A comparison of the vertical displacements at 90 psi for Shot Cactus (Gage 22, Station 125.09) and at 84 psi for Shot Koa (Gage 23, Station 125.05) shows that the displacements for Shot Koa are higher in the low-frequency range (twice as high at 3 cps), lower for the intermediate-frequency range (10 to 50 cps) and about equal for the high-frequency range (Figures 21 and 32).

The radial displacements for Shot Cactus at 90 psi (Gage 13, Station 125.09) are about the same as for Shot Koa at 84 psi (Gage 19, Station 125.05) except in an intermediate-frequency range (10 to 50 cps) where the Shot Cactus values are greater (Figures 22 and 39).

CONCLUSIONS

High-frequency gages (3 to 300 cps) gave readable records with excellent consistency of values in duplicate installations.

Low-frequency gages (3 to 10 cps), which were designed for much higher displacements than observed, produced records with considerable scatter.

In general, vertical and radial displacements for the high-yield shot were much lower than expected from the extrapolation of Plumbbob data. Differences in soil conditions, surface versus raised bursts, and topography variations may have been contributing factors.

A brief outline of separate parametric analyses and theoretical studies, published as Reference 8, is given in the Appendix.

Appendix
DISPLACEMENT SHOCK SPECTRA VELOCITY, and ACCELERATION of a HALF-SPACE in RESPONSE to a MOVING PRESSURE PULSE - GENERAL OUTLINE

INTRODUCTION

In this study, the following conditions are assumed to exist in the soil, near the ground level, exposed to a nuclear explosion.

1. The soil is homogeneous, isotropic, and elastic.
2. The point under investigation is far enough away from the explosion so that the radius of curvature of the shock-wave front is large compared with the dimensions of the soil body considered.
3. For the size of soil body considered, the shock wave appears as a steadily moving pressure pulse whose intensity and geometric distribution are invariant. (This assumption has been eliminated in later studies; the theory is presented in Reference 12. Because the numerical calculations based on these later studies have not yet been completed, none of the results are presented here.)

Under these assumptions the soil-response problem may be approximated by a two-dimensional problem in which an invariant pressure pulse moves with a constant speed over an elastic half space. Future studies will deal with the effects of soil layering, solid bodies enclosed in the soil, nonlinear visco-elastic or plastic and compactible soils, three-dimensional effects, coupling of air and soil, and the like.

The problem of a steadily moving line load over elastic half space was formulated and solved by Lamb, Sneddon, Huth, and Cole (References 9, 10, and 11). The simplicity of the problem and the applications of the solution to shock-spectrum studies are demonstrated below.

THE MATHEMATICAL PROBLEM

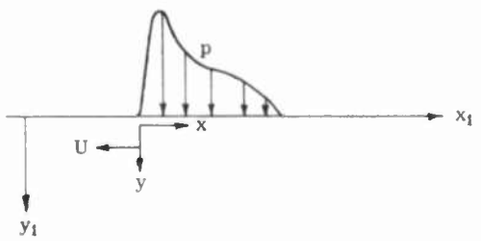

Let x_1, y_1 be space coordinates fixed in the medium which occupies the half space $y_1 > 0$ and let x and y be coordinates which move at the constant speed of the pressure pulse U in the negative x_1 direction. The medium is assumed to obey Hooke's law

$$\sigma_{ij} = \lambda e_{mm}\delta_{ij} + 2\mu e_{ij} \qquad (A.1)$$

where λ and μ are Lamé are constants. The equation of motion is then, in vector notation

$$(\lambda + 2\mu)\nabla(\nabla \cdot \vec{u}) - \mu\nabla \times (\nabla \times \vec{u}) = \rho \frac{\partial^2 \vec{u}}{\partial t^2} . \qquad (A.2)$$

where $\vec{u}(u, v)$ is the displacement vector. If the displacement is separated into a dilatational and rotational part, so that, in the plane-strain case under consideration,

$$u = \frac{\partial \phi}{\partial x_1} - \frac{\partial \psi}{\partial y_1} \qquad v = \frac{\partial \phi}{\partial y_1} + \frac{\partial \psi}{\partial x_1} \qquad (A.3)$$

a solution is obtained, provided ϕ and ψ satisfy the equations

$$\begin{aligned} \phi_{x_1x_1} + \phi_{y_1y_1} &= \frac{1}{a_1^2}\phi_{tt} \\ \psi_{x_1x_1} + \psi_{y_1y_1} &= \frac{1}{a_2^2}\psi_{tt} \end{aligned} \qquad (A.4)$$

where

$$a_1 = \sqrt{\frac{\lambda + 2\mu}{\rho}} \qquad a_2 = \sqrt{\frac{\mu}{\rho}} \qquad (A.5)$$

a_1 and a_2 are the dilatational and shear wave speeds in the medium, respectively. In the plane-strain case, the stress components are

$$\begin{aligned} \sigma_{x_1} &= (\lambda + 2\mu)u_{x_1} + \lambda v_{y_1} \\ \sigma_{y_1} &= \lambda u_{x_1} + (\lambda + 2\mu)v_{y_1} \\ \tau_{x_1y_1} &= \mu(u_{y_1} + v_{x_1}) \end{aligned} \qquad (A.6)$$

In the above problem, the pressure pulse is considered as a function of x + Ut only. Hence, with a Galilean transformation

$$x = x_1 + Ut \qquad y = y_1 \tag{A.7}$$

and the boundary conditions are

$$\sigma_y = -p(x) \qquad \tau_{xy} = 0 \qquad \text{when} \quad y = 0 \tag{A.8}$$

which is independent of the time t. In the steady state, the differential Equations A.4 are transformed by A.7 into

$$\phi_{xx} + \phi_{yy} + \frac{U^2}{a_1^2}\phi_{xx}$$

$$\psi_{xx} + \psi_{yy} = \frac{U^2}{a_2^2}\psi_{xx} \tag{A.9}$$

or, introducing the Mach numbers,

$$M_1 = \frac{U}{a_1} \qquad M_2 = \frac{U}{a_2} \tag{A.10}$$

and the parameters,

$$\beta_1 = \sqrt{1 - M_1^2} \qquad \beta_2 = \sqrt{1 - M_2^2} \tag{A.11}$$

if $M_1, M_2 < 1$

and

$$\bar{\beta}_1 = \sqrt{M_1^2 - 1} \qquad \bar{\beta}_2 = \sqrt{M_2^2 - 1} \tag{A.12}$$

if $M_1, M_2 > 1$

the elliptic equations are

$$\beta_1^2 \phi_{xx} + \phi_{yy} = 0 \quad \text{if } M_1 < 1$$

$$\beta_2^2 \psi_{xx} + \psi_{yy} = 0 \quad \text{if } M_2 < 1 \tag{A.13}$$

and the hyperbolic equations are

$$\bar{\beta}_1^2 \phi_{xx} - \phi_{yy} = 0 \quad \text{if } M_1 > 1$$

$$\bar{\beta}_1^2 \psi_{xx} - \psi_{yy} = 0 \quad \text{if } M_2 > 1 \tag{A.14}$$

Expressions for the stress components may be reduced, by means of Equations A.9 and A.10 into

$$\frac{\sigma_x}{\mu} = (M_2^2 - 2M_1^2 + 2)\phi_{xx} - 2\psi_{xy}$$

$$\frac{\sigma_y}{\mu} = (M_2^2 - 2)\phi_{xx} + 2\psi_{xy} \tag{A.15}$$

$$\frac{\tau_{xy}}{\mu} = 2\phi_{xy} - (M_2^2 - 2)\psi_{xx}$$

The boundary conditions (Equation A.8) can be integrated once to obtain, at $y = 0$,

$$(M_2^2 - 2)\phi_x + 2\psi_y = -\frac{1}{\mu}\int_0^x p(x)dx$$

$$2\phi_y - (M_2^2 - 2)\psi_x = 0 \tag{A.16}$$

When ϕ and ψ are solved from Equations A.13 or A.14 with the boundary conditions (Equation A.16) on the free surface and suitable radiation and finiteness conditions at infinity are satisfied, the displacements u and v can be obtained from Equation A.3, the stresses σ_x, σ_y, and τ_{xy} can be obtained from Equation A.15, and the velocity and acceleration with respect to the space coordinates fixed in the medium by

$$\frac{\partial u}{\partial t} = U\frac{\partial u}{\partial x_1} = U(\phi_x - \psi_y)_x$$

$$\frac{\partial v}{\partial t} = U\frac{\partial v}{\partial x_1} = U(\phi_y + \psi_x)_x$$

$$\frac{\partial^2 u}{\partial t^2} = U^2\frac{\partial^2 u}{\partial x_1^2} = U^2(\phi_x - \psi_y)_{xx} \tag{A.17}$$

$$\frac{\partial^2 v}{\partial t^2} = U^2\frac{\partial^2 v}{\partial x_1^2} = U^2(\phi_y + \psi_x)_{xx}$$

With the same steps as in Reference 11, it is possible to obtain the following ground acceierations at any depth, $y = UY$, and any time t in the horizontal ($\ddot{u}$) and vertical ($\ddot{v}$) directions due to an invariant pressure

$p(t) = p_m p_1(t)$, where p_m = peak overpressure.

PRESSURE PULSE MOVING FASTER THAN DILATATIONAL OR SHEAR SPEED ($M_2 > M_1 > 1$, SUPERSONIC)

$$\frac{\rho a_1}{p_m}\ddot{u} = -\frac{C_1}{\bar{\beta}_1}p_1'(t - \bar{\beta}_1 Y) + \bar{\beta}_2 C_2 p_1'(t - \bar{\beta}_2 Y) \tag{A.18}$$

$$\frac{\rho a_1}{p_m}\ddot{v} = C_1 p_1'(t - \bar{\beta}_1 Y) + C_2 p_1'(t - \bar{\beta}_2 Y)$$

where primes indicate the derivatives of the pressure-pulse curve with respect to the argument and

$$C_1 = M_1\left(\frac{M_2}{M_1}\right)^2 \frac{\bar{\beta}_1\left(\bar{\beta}_2^2 - 1\right)}{\left(\bar{\beta}_2^2 - 1\right)^2 + 4\bar{\beta}_1\bar{\beta}_2} \tag{A.19}$$

$$C_2 = M_1\left(\frac{M_2}{M_1}\right)^2 \quad \frac{2\bar{\beta}_1}{\left(\bar{\beta}_2^2 - 1\right)^2 + 4\bar{\beta}_1\bar{\beta}_2}$$

PRESSURE PULSE MOVING FASTER THAN SHEAR WAVES AND SLOWER THAN DILATATIONAL WAVES ($M_2 > 1 > M_1$, TRANSONIC)

$$\frac{\rho a_1}{p_m}\ddot{u} = \frac{C_6}{\beta_1}\left(U^2\frac{d^2I_1}{dx^2}\right) + \frac{C_5}{\beta_1}\left(U^2\frac{d^2H_1}{dx^2}\right) + \bar{\beta}_2 C_7\left(U^2\frac{d^2N_3}{dx^2}\right) + \bar{\beta}_2 C_8\left(U^2\frac{d^2N_4}{dx^2}\right) \tag{A.20}$$

$$\frac{\rho a_1}{p_m}\ddot{v} = -C_5\left(U^2\frac{d^2I_1}{dx^2}\right) + C_6\left(U^2\frac{d^2H_1}{dx^2}\right) + C_7\left(U^2\frac{d^2N_3}{dx^2}\right) + C_8\left(U^2\frac{d^2N_4}{dx^2}\right)$$

where

$$C_5 = \frac{M_1}{\pi}\left(\frac{M_2}{M_1}\right)^2 \quad \frac{\beta_1\left(1-\bar{\beta}_2^2\right)^3}{\left(1-\bar{\beta}_2^2\right)^4 + 16\beta_1^2\bar{\beta}_2^2}$$

$$C_8 = -\frac{M_1}{\pi}\left(\frac{M_2}{M_1}\right)^2 \frac{4\beta_1^2\bar{\beta}_2\left(1-\bar{\beta}_2^2\right)}{\left(1-\bar{\beta}_2^2\right)^4 + 16\beta_1^2\bar{\beta}_2^2} \tag{A.21}$$

$$C_7 = \frac{M_1}{\pi}\left(\frac{M_2}{M_1}\right)^2 \frac{2\beta_1\left(1-\bar{\beta}_2^2\right)^2}{\left(1-\bar{\beta}_2^2\right)^4 + 16\beta_1^2\bar{\beta}_2^2}$$

$$C_8 = M_1\left(\frac{M_2}{M_1}\right)^2 \frac{8\beta_1^2\bar{\beta}_2}{\left(1-\bar{\beta}_2^2\right)^4 + 16\beta_1^2\bar{\beta}_2^2}$$

$$\left(U^2\frac{d^2I_1}{dx^2}\right) = \frac{tp_1(o)}{t^2+\beta_1^2Y^2} + \int_o^t p \frac{t-\tau}{(t-\tau)^2+\beta_1^2Y^2} p_1'(\tau)d\tau$$

$$\left(U^2\frac{d^2H_1}{dx^2}\right) = \frac{\beta_1 Y p_1(o)}{t^2+\beta_1^2Y^2} + \int_o^t p \frac{\beta_1 Y}{(t-\tau)^2+\beta_1^2Y^2} p_1'(\tau)d\tau$$

$$= p_1(t) \quad , \ \beta_1 \neq 0$$

$$, \ \beta_1 = 0$$

$$\left(U^2\frac{d^2N_3}{dx^2}\right) = \frac{p_1(o)}{t-\bar{\beta}_2 Y} + \int_o^t p \frac{p_1'(\tau)d\tau}{t-\tau-\bar{\beta}_2 Y} \tag{A.22}$$

$$\left(U^2\frac{d^2N_4}{dx^2}\right) = p_1'(t-\bar{\beta}_2 Y)$$

PRESSURE PULSE MOVING SLOWER THAN SHEAR OR DILATATIONAL WAVES ($1 > M_2 > M_1$, SUBSONIC)

$$\frac{\rho a_1}{p_m}\ddot{u} = \frac{C_4}{\beta_1}\left(U^2\frac{d^2H_1}{dx^2}\right) - \beta_2 C_3\left(U^2\frac{d^2H_2}{dx^2}\right) \tag{A.23}$$

$$\frac{\rho a_1}{p_m}\ddot{v} = C_3\left(U^2\frac{d^2I_2}{dx^2}\right) - C_4\left(U^2\frac{d^2I_1}{dx^2}\right)$$

where

$$C_3 = \frac{M_1}{\pi}\left(\frac{M_2}{M_1}\right)^2 \quad \frac{2\beta_1}{\left(1+\beta_2^2\right)^2 - 4\beta_1\beta_2} \tag{A.24}$$

$$C_4 = \frac{M_1}{\pi}\left(\frac{M_2}{M_1}\right)^2 \quad \frac{\beta_1\left(1+\beta_2\right)^2}{\left(1+\beta_2^2\right)^2 - 4\beta_1\beta_2}$$

SHOCK-SPECTRA CALCULATIONS

Shock spectra show the peak response of a single-degree-of-freedom system relative to the ground, due to the ground motion, as a function of the frequency of the single-degree-of-freedom system attached to the ground. That is D_{max} (maximum displacement) is the maximum value of the solution of the differential equation

$$\ddot{q} + \omega^2 q = -a(t) \qquad (A.25)$$

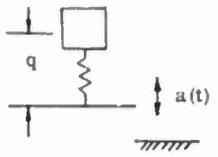

where a(t) is the acceleration of the support. For this study various pressure-pulse curves were taken and the resulting ground-acceleration time history for various depths computed. These ground accelerations were then introduced in place of a(t) in Equation A.25, and the peak responses were determined.

Figure A.1 summarizes the range of parameters investigated. The straight lines represent constant ratios of M_2/M_1 or a_1/a_2 which correspond to constant Poisson ratios of the elastic half space. The three regions of interest are designated by subsonic ($1 > M_2 > M_1$), transonic ($M_2 > 1 > M_1$) and supersonic ($M_2 > M_1 > 1$). The range of parameters investigated was $0 < M_1 < 2$ and $0 < y < 100$ for Poisson ratios of 0.25 and 0.45.

Some typical results from the steady-state solution are shown in Figures A.2 through A.5 where a theoretical curve has been superimposed on plots of data from the Hardtack and Plumbbob tests. These theoretical curves were based on yields of 40 kt and 2 Mt, in the 100-psi-overpressure region. The calculations were carried out for a triangular pressure-pulse approximation of Brode's theoretical pressure pulse by choosing the duration of the triangular pressure-pulse curve so that the area under the curve was equal to the positive phase of Brode's theoretical curve. The theoretical shock-spectra curves shown were based on a soil with dilatational speed, a_1 = 1,500 ft/sec, Poisson ratio, ν = 0.45, soil density = 100 lb/ft^3, and depth = 5 ft. At this 100-psi-overpressure location, the blast wave velocity of U = 3,000 ft/sec is larger than either seismic speed and, therefore, corresponds to the supersonic case. It should be noted that, in general, the theoretical curves underestimate the measured data. Since the shock spectra vary nearly inversely with ρa_1 in this range of U/a_1 values, a smaller value of ρa_1 will shift the theoretical curve upward and bring it into closer agreement with the data.

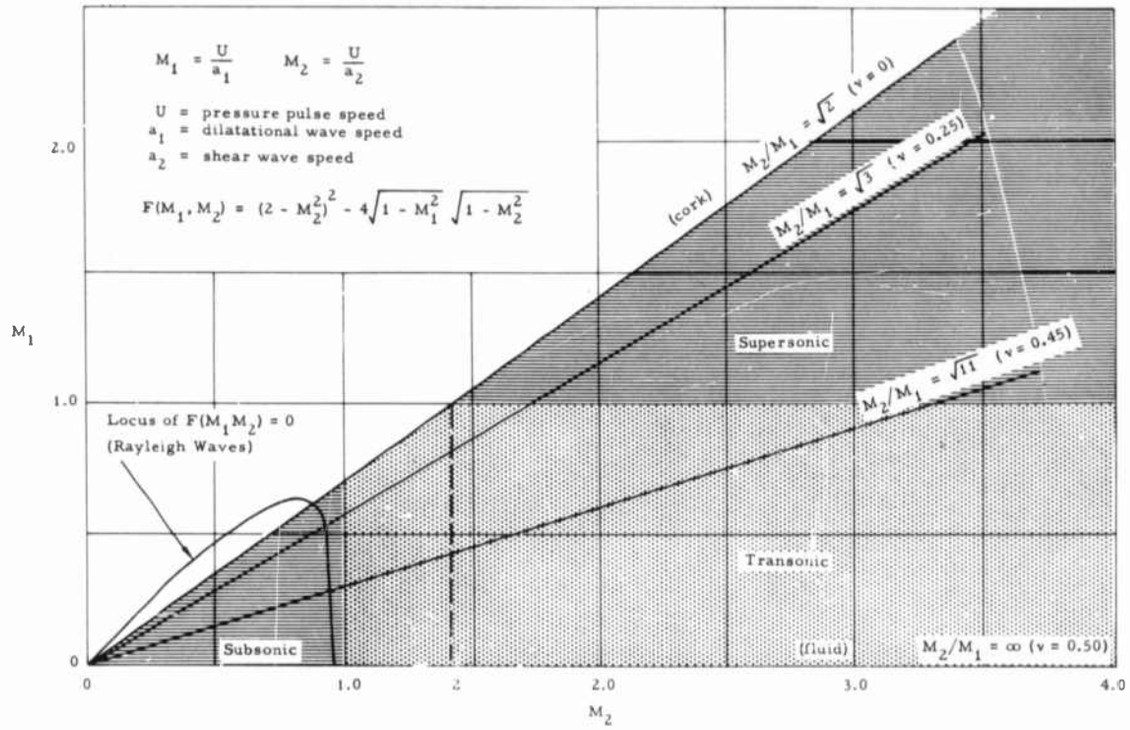

Figure A.1 Ground shock studies, summary of cases.

In these calculations, the value of 100 lb/ft^3 for soil density may be slightly high. In addition, the seismic speed of a_1 = 1,500 ft/sec is certainly high as compared with the values measured close to the surface during Operation Hardtack, where some measured values were as low as 800 ft/sec. However, seismic measurements showed that the seismic speed increased rapidly with increasing depth near the water table, which was at about 20 feet. This, of course, makes it difficult to pick a representative seismic speed to be

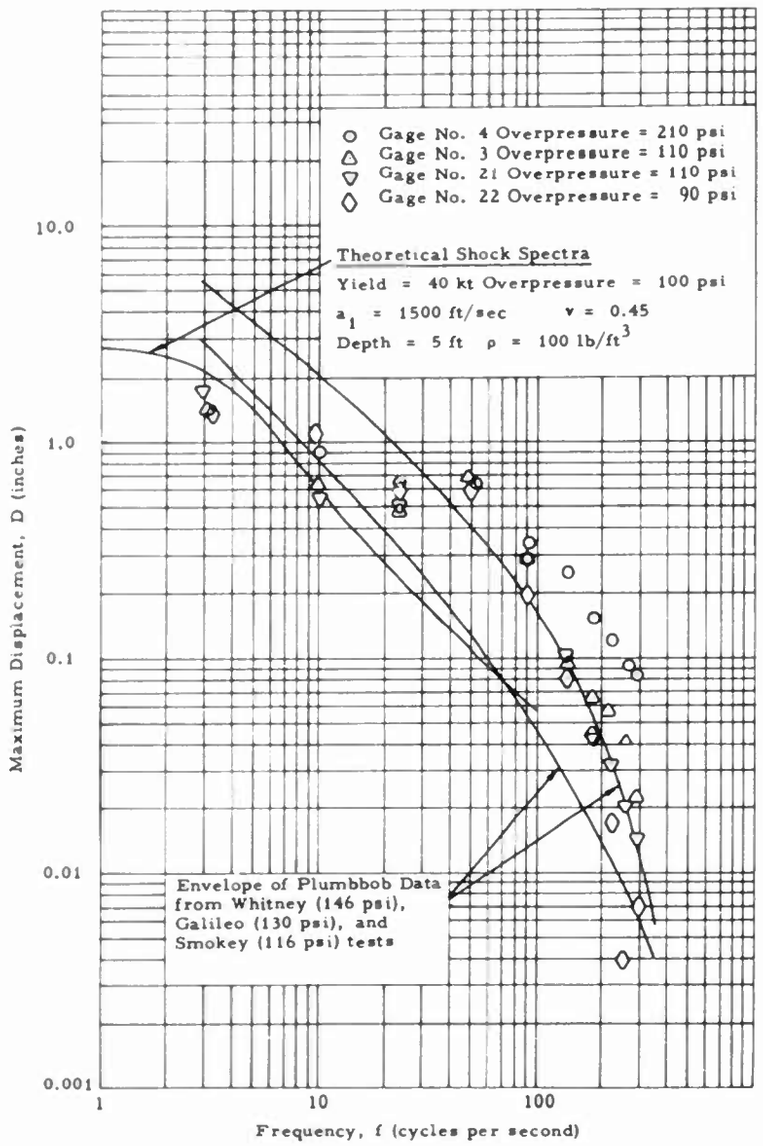

Figure A.2 Displacement shock spectrum, vertical direction, Shot Cactus.

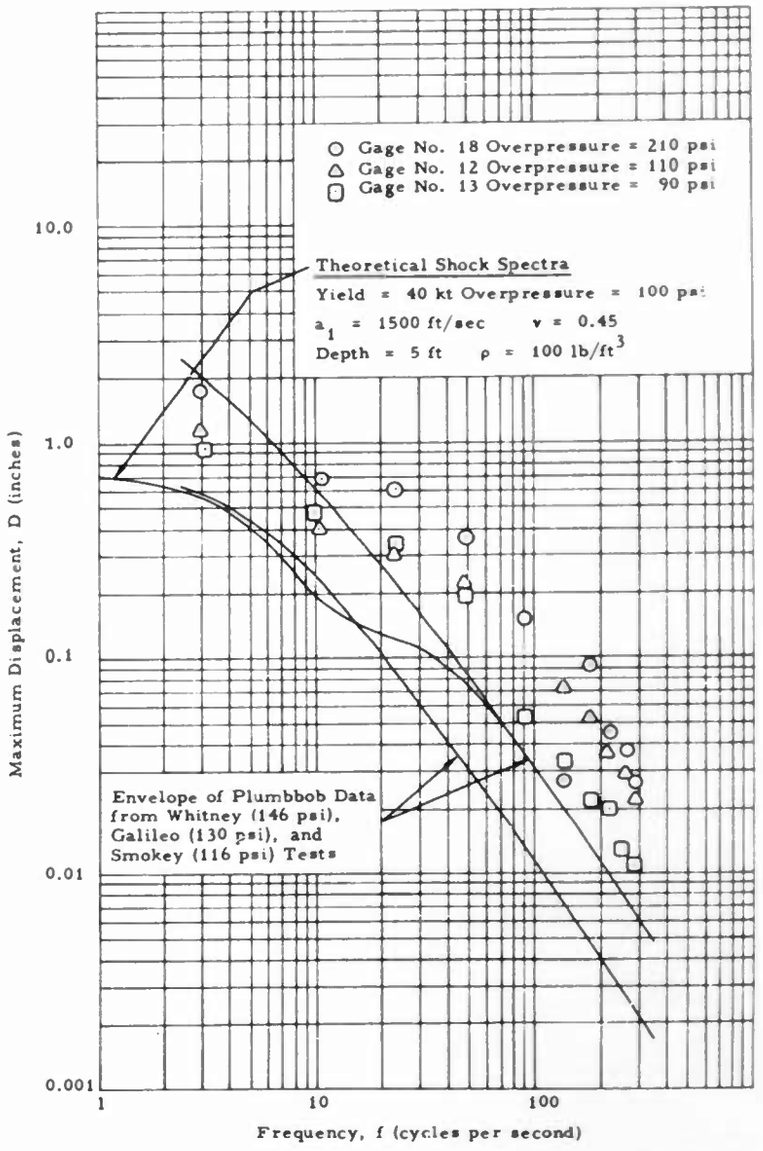

Figure A.3 Displacement shock spectrum, radial direction, Shot Cactus.

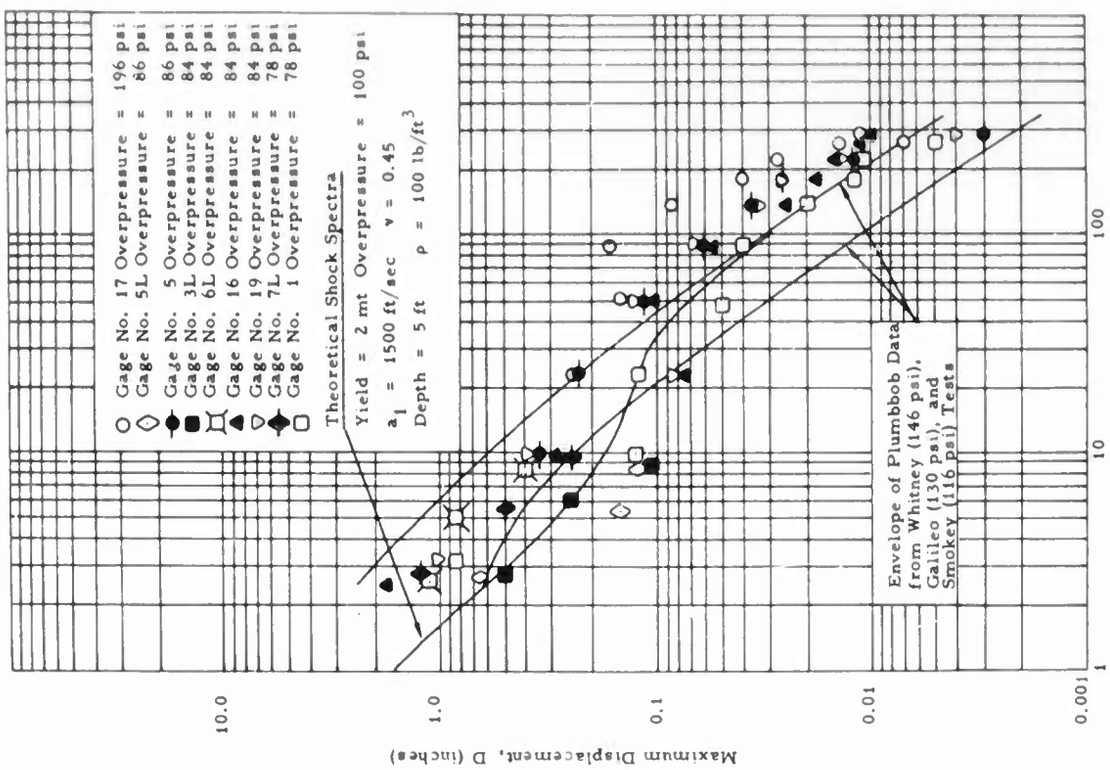

Figure A.5 Displacement shock spectrum, radial direction, Shot Koa.

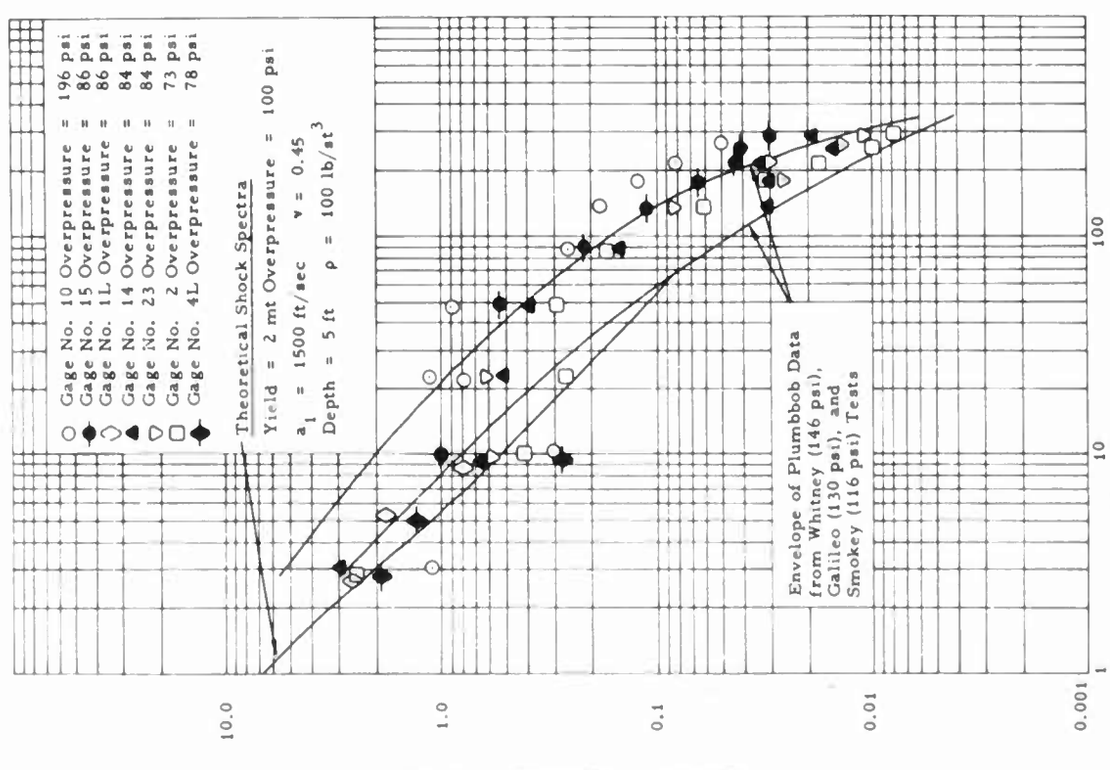

Figure A.4 Displacement shock spectrum, vertical direction, Shot Koa.

used in this theoretical study. If, for example, the seismic speed of 1,000 ft/sec was used in place of the value of 1,500 ft/sec, then the theoretical shock-spectra curve would be shifted upward by a factor of 1,500/1,000 = 1.5, bringing the theoretical curve into much closer agreement with the measured data.

It should be mentioned that since there is no data available from which the Poisson ratio can be determined for either the Hardtack or Plumbbob test sites, a search of the literature was made to determine a representative value of the Poisson ratio for a typical soil. In Reference 14, the shear and dilatational wave speeds were measured in Pierre shale in eastern Colorado. From these speeds, the Poisson ratio is calculated to be 0.415 and 0.419 in the vertical and horizontal directions, respectively. In Reference 13, the shear and dilatational wave speeds were measured in Eagle Ford shale and Austin chalk in Dallas County, Texas. From these speeds, Poisson's ratio was calculated to be 0.47 and 0.46 in the vertical and horizontal directions, respectively, for the Eagle Ford shale and 0.40 and 0.41 in the vertical and horizontal directions, respectively, for the Austin chalk. From these references, it appears that the theoretical shock spectra calculated using the Poisson ratio of 0.45 is more representative for a soil than the spectra calculated using the Poisson ratio of 0.25.

An examination of the expressions for the ground accelerations show that in the subsonic case, the denominator of C_3 and C_4 may be zero for certain values of the seismic speeds a_1 and a_2. Herein lies one serious defect with the steady-state solution. In this case the pressure-pulse speed U is moving over the half space (the earth) at the same speed at which Rayleigh surface waves are propagated within the half space and, therefore, a type of resonance exists. Of course, in a real situation this would not occur, because U is not constant, but rather, decreases with time. Hence the air-wave speed would pass through the Rayleigh wave speed and would cause large but finite ground motions at a distance from the explosion where the speed of the wave front has slowed down to the Rayleigh-wave speed. (This, of course, assumes that the speed of the wave front at the epicenter is larger than the Rayleigh-wave speed in the elastic half space.) Thus the shock spectrum cannot be computed when the Rayleigh-wave speed coincides with the blast-wave speed or is in some "neighborhood" of speeds "close" to the Rayleigh-wave speeds. As a result of this defect in the steady-state solution, another study has been undertaken in which the blast-wave speed U is no longer constant but decreases with increasing distance from the epicenter. The theoretical work of this study is reported in Reference 12. The study indicated that the steady-state solution herein reported is a good approximation of the transient solution for blast-wave speeds "sufficiently far" from the Rayleigh-wave speeds. Shock-spectrum calculations based on the transient solution of Reference 12 have not been completed to date. The results of these calculations will be presented in an STL report at the completion of the investigation.

REFERENCES

1. J. F. Halsey and M. V. Barton; "Spectra of Ground Shocks Produced by Nuclear Detonations"; Project 1.9, Operation Plumbbob, WT-1487, August 1959; Air Force Ballistic Missile Division, Air Research and Development Command, Los Angeles 45, California; Confidential.

2. M. V. Barton; "Ground Shock Measurements and Structural Response"; GM-TR-293, 11 December 1957; The Ramo-Wooldridge Corporation, Los Angeles 45, California; Confidential.

3. M. V. Barton; "Ground Shock Specifications"; GM 61.0-176, 6 February 1958 (Amended); The Ramo-Wooldridge Corporation, Los Angeles 45, California; Confidential.

4. Y. C. Fung and M. V. Barton; "Some Characteristics and Uses of Shock Spectra"; GM-TR-82, 15 October 1956; The Ramo-Wooldridge Corporation, Los Angeles 45, California; Unclassified.

5. G. W. Housner and G. D. McCann; "The Analysis of Strong-Motion Earthquakes Records with the Electric Analog Computer"; Bulletin Selsmological Society of America; Volume 39, No. 1, January 1949; Unclassified.

6. G. W. Housner, R. R. Martel, and J. L. Alfrod; "Spectrum Analysis of Strong Motion Earthquakes"; Bulletin Seismological Society of America; Volume 43, No. 2, April 1953; Unclassified.

7. Y. C. Fung; "On the Safety of Structures Against Ground Shocks"; GM-TR-191, 15 June 1957; The Ramo-Wooldridge Corporation, Los Angeles 45, California; Unclassified.

8. R. E. Hutton; "Displacement Shock Spectra, Velocity, and Acceleration of a Half-Space In Response to a Moving Pressure Pulse"; EM 9-21, September 1957; Space Technology Laboratories, Inc., Los Angeles 45, California; Confidential.

9. H. Lamb; "On Waves Due to a Traveling Disturbance, with Application to Waves In Superposed Fluids"; Phil. Mag. (6), Vol. 13, pp 386-399; 1916.

10. I. N. Sneddon; "Stress Produced by a Pulse of Pressure Moving Along the Surface of a Semi-infinite Solid"; Rend, Circ. Matematico di Palermo, (2), Vol. 1, pp 57-62; Jan-April 1952.

11. J. D. Cole and J. H. Huth; "Elastic Stresses Produced in a Half-Plane by Steadily Moving Loads." Paper presented at the 9th International Congress of Applied Mechanics In Brussels, 1956. The Rand Corporation Report P-884.

12. J. W. Miles; "On the Response of an Elastic Half-Space to a Moving Blast Wave"; GM-TR-0165-00524, 24 November 1958; Space Technology Laboratories, Inc., Los Angeles 45, California.

13. J. White and R. Sengbush; "Velocity Measurements in Near-Surface Formations"; Geophysics, No. 1, January 1953.

14. R. Sengbush and others; "Attenuation of Shear and Compressional Waves in Pierre Shale"; Geophysical Prospecting, Vol. VI, No. 4, December 1958.

DISTRIBUTION

Military Distribution Category 14

ARMY ACTIVITIES

1 Deputy Chief of Staff for Military Operations, D/A, Washington 25, D.C. ATTN: Dir. of SW&R
2 Chief of Research and Development, D/A, Washington 25, D.C. ATTN: Atomic Div.
3 Assistant Chief of Staff, Intelligence, D/A, Washington 25, D.C.
4 Chief of Engineers, D/A, Washington 25, D.C. ATTN: ENGNB
5 Chief of Engineers, D/A, Washington 25, D.C. ATTN: ENGEB
6 Chief of Engineers, D/A, Washington 25, D.C. ATTN: ENGTB
7- 8 Office, Chief of Ordnance, D/A, Washington 25, D.C. ATTN: ORDTN
9- 11 Commanding General, U.S. Continental Army Command, Ft. Monroe, Va.
12 Director of Special Weapons Development Office, Headquarters CONARC, Ft. Bliss, Tex. ATTN: Capt. Chester I. Petereon
13 President, U.S. Army Artillery Board, Ft. Sill, Okla.
14 President, U.S. Army Air Defense Board, Ft. Bliss, Tex.
15 Commandant, U.S. Army Command & General Staff College, Ft. Leavenworth, Kansas. ATTN: ARCHIVES
16 Commandant, U.S. Army Air Defense School, Ft. Bliss, Tex. ATTN: Command & Staff Dept.
17 Commandant, U.S. Army Armored School, Ft. Knox, Ky.
18 Commandant, U.S. Army Artillery and Missile School, Ft. Sill, Okla. ATTN: Combat Development Department
19 Commandant, U.S. Army Aviation School, Ft. Rucker, Ala.
20 Commandant, U.S. Army Infantry School, Ft. Benning, Ga. ATTN: C.D.S.
21 Commandant, U.S. Army Ordnance School, Aberdeen Proving Ground, Md.
22 Commandant, U.S. Army Ordnance and Guided Missile School, Redstone Arsenal, Ala.
23 Commanding General, Chemical Corps Training Comd., Ft. McClellan, Ala.
24 Commanding General, The Engineer Center, Ft. Belvoir, Va. ATTN: Asst. Cmdt, Engr. School
25 Director, Armed Forces Institute of Pathology, Walter Reed Army Med. Center, 625 16th St., NW, Washington 25, D.C.
26 Commanding Officer, Army Medical Research Lab., Ft. Knox, Ky.
27 Commandant, Walter Reed Army Inst. of Res., Walter Reed Army Medical Center, Washington 25, D.C.
28- 29 Commanding General, Qm R&D Comd., QM R&D Cntr., Natick, Mass. ATTN: CBR Liaison Officer
30- 31 Commanding Officer, Chemical Warfare Lab., Army Chemical Center, Md. ATTN: Tech. Library
32 Commanding General, Engineer Research and Dev. Lab., Ft. Belvoir, Va. ATTN: Chief, Tech. Support Branch
33 Director, Waterways Experiment Station, P.O. Box 631, Vicksburg, Miss. ATTN: Library
34 Commanding Officer, Picatinny Arsenal, Dover, N.J. ATTN: ORDBB-TK
35 Commanding Officer, Diamond Ord. Fuze Labs., Washington 25, D.C. ATTN: Chief, Nuclear Vulnerability Br. (230)
36- 37 Commanding General, Aberdeen Proving Grounds, Md. ATTN: Director, Ballistics Research Laboratory
38 Commander, Army Rocket and Guided Missile Agency, Redstone Arsenal, Ala. ATTN: Tech Library
39 Commanding General, White Sands Proving Ground, Las Cruces, N. Mex. ATTN: ORDBS-OM
40 Commander, Army Ballistic Missile Agency, Redstone Arsenal, Ala. ATTN: ORDAB-HT
41 Commanding General, U.S. Army Electronic Proving Ground, Ft. Huachuca, Ariz. ATTN: Tech. Library
42 Commanding General, USA Combat Surveillance Agency, 1124 N. Highland St., Arlington, Va.
43 Director, Operations Research Office, Johns Hopkins University, 6935 Arlington Rd., Bethesda 14, Md.
44 Commanding General, U. S. ORD Special Weapons-Ammunition Command, Dover, N.J.
45 Commander-in-Chief, U.S. Army Europe, APO 403, New York, N.Y. ATTN: Opot. Div., Weapons Br.

NAVY ACTIVITIES

46 Chief of Naval Operations, D/N, Washington 25, D.C. ATTN: OP-03EG
47 Chief of Naval Operations, D/N, Washington 25, D.C. ATTN: OP-75
48- 49 Chief of Naval Research, D/N, Washington 25, D.C. ATTN: Code 811
50- 52 Chief, Bureau of Naval Weapons, D/N, Washington 25, D.C. ATTN: DLI-3
53 Chief, Bureau of Ordnance, D/N, Washington 25, D.C.
54 Chief, Bureau of Ships, D/N, Washington 25, D.C. ATTN: Code 423
55 Chief, Bureau of Yards and Docks, D/N, Washington 25, D.C. ATTN: D-440
56 Director, U.S. Naval Research Laboratory, Washington 25, D.C. ATTN: Mrs. Katherine H. Cass
57- 58 Commander, U.S. Naval Ordnance Laboratory, White Oak, Silver Spring 19, Md.
59 Commanding Officer and Director, Navy Electronics Laboratory, San Diego 52, Calif.
60 Commanding Officer, U.S. Naval Mine Defense Lab., Panama City, Fla.
61- 62 Commanding Officer, U.S. Naval Radiological Defense Laboratory, San Francisco, Calif. ATTN: Tech. Info. Div.
63- 64 Commanding Officer and Director, U.S. Naval Civil Engineering Laboratory, Port Hueneme, Calif. ATTN: Code L31
65 Commanding Officer, U.S. Naval Schools Command, U.S. Naval Station, Treasure Island, San Francisco, Calif.
66 Superintendent, U.S. Naval Postgraduate School, Monterey, Calif.
67 Commanding Officer, U.S. Fleet Sonar School, U.S. Naval Base, Key West, Fla.
68 Officer-in-Charge, U.S. Naval School, CEC Officers, U.S. Naval Construction Bn. Center, Port Hueneme, Calif.
69 Commanding Officer, Nuclear Weapons Training Center, Atlantic, U.S. Naval Base, Norfolk 11, Va. ATTN: Nuclear Warfare Dept.
70 Commanding Officer, Nuclear Weapons Training Center, Pacific, Naval Station, San Diego, Calif.
71 Commanding Officer, U.S. Naval Damage Control Tng. Center, Naval Base, Philadelphia 12, Pa. ATTN: ABC Defense Course
72 Commanding Officer, Naval Air Material Center, Philadelphia 12, Pa. ATTN: Technical Data Br.
73 Commanding Officer, U.S. Naval Air Development Center, Johnsville, Pa. ATTN: NAS, Librarian
74 Commanding Officer, U.S. Naval Medical Research Institute, National Naval Medical Center, Bethesda, Md.
75 Commanding Officer and Director, David W. Taylor Model Basin, Washington 7, D.C. ATTN: Library
76 Commanding Officer and Director, U.S. Naval Engineering Experiment Station, Annapolis, Md.
77 Commander, Norfolk Naval Shipyard, Portsmouth, Va. ATTN: Underwater Explosions Research Division
78 Commandant, U.S. Marine Corps, Washington 25, D.C. ATTN: Code A03H
79 Director, Marine Corps Landing Force, Development Center, MCS, Quantico, Va.

80 Commanding Officer, U.S. Naval CIC School, U.S. Naval Air Station, Glynco, Brunswick, Ga.
81- 83 Chief, Bureau of Naval Weapons, Navy Department, Washington 25, D.C. ATTN: RR12

AIR FORCE ACTIVITIES

84 Hq. USAF, ATTN: Operations Analysis Office, Office, Vice Chief of Staff, Washington 25, D. C.
85- 86 Air Force Intelligence Center, HQ. USAF, ACS/I (AFCIN-3V1) Washington 25, D.C.
87 Director of Research and Development, DCS/D, HQ. USAF, Washington 25, D.C. ATTN: Guidence and Weapons Div.
88 The Surgeon General, HQ. USAF, Washington 25, D.C. ATTN: Bio.-Def. Pre. Med. Division
89 Commander, Tactical Air Command, Langley AFB, Va. ATTN: Doc. Security Branch
90 Commander, Air Defense Command, Ent AFB, Coloredo. ATTN: Assistant for Atomic Energy, ADLDC-A
91 Commandar, Hq. Air Research and Development Command, Andrews AFB, Washington 25, D.C. ATTN: RDRWA
92 Commander, Air Force Ballistic Missile Div. HQ. ARDC, Air Force Unit Post Office, Los Angeles 45, Calif. ATTN: WDSOT
93- 94 Commander, AF Cambridge Research Center, L. G. Hanscom Field, Bedford, Mass. ATTN: CRQST-2
95- 99 Commander, Air Force Special Weapons Center, Kirtland AFB, Albuquerque, N. Mex. ATTN: Tech. Info. & Intel. Div.
100-101 Director, Air University Library, Maxwell AFB, Ala.
102 Commander, Lowry Technical Training Center (TW), Lowry AFB, Denver, Coloredo.
103 Commandant, School of Aviation Medicine, Brooks Air Force Base, Tex. ATTN: Research Secretariat
104 Commander, 1009th Sp. Wpns. Squadron, HQ. USAF, Washington 25, D.C.
105-107 Commander, Wright Air Development Center, Wright-Patterson AFB, Dayton, Ohio. ATTN: WCACT (For WCOSI)
108-109 Director, USAF Project RAND, VIA: USAF Liaison Office, The RAND Corp., 1700 Main St., Santa Monica, Calif.
110 Commander, Rome Air Development Center, ARDC, Griffiss AFB, N.Y. ATTN: Documents Library, RCSSL-1
111 Commander, Air Technical Intelligence Center, USAF, Wright-Patterson AFB, Ohio. ATTN: AFCIN-4Ble, Library
112 Headquarters, 1st Missile Div., USAF, Vandenberg AFB, Calif. ATTN: Operations Analysis Office
113 Assistant Chief of Staff, Intelligence, HQ. USAFE, APO 633, New York, N.Y. ATTN: Directorate of Air Targets
114 Commander-in-Chief, Pacific Air Forces, APO 953, San Francisco, Calif. ATTN: PFCIE-MB, Base Recovery

OTHER DEPARTMENT OF DEFENSE ACTIVITIES

115 Director of Defense Research and Engineering, Washington 25, D.C. ATTN: Tech. Library
116 Chairman, Armed Services Explosives Safety Board, DOD, Building T-7, Grevelly Point, Washington 25, D.C.
117 Director, Weapons Systems Evaluation Group, Room 1E880, The Pentagon, Washington 25, D.C.
118-121 Chief, Defense Atomic Support Agency, Washington 25, D.C. ATTN: Document Library
122 Commander, Field Command, DASA, Sandia Base, Albuquerque, N. Mex.
123-124 Commander, Field Command, DASA, Sandia Base, Albuquerque, N. Mex. ATTN: FCTG
125-126 Commander, Field Command, DASA, Sandia Base, Albuquerque, N. Mex. ATTN: FCWT
127 Commander, JTF-7, Arlington Hall Station, Arlington 12, Va.
128 Commander-in-Chief, Strategic Air Command, Offutt AFB, Neb. ATTN: OAWS
129 U.S. Documents Officer, Office of the United States National Military Representative - SHAPE, APO 55, New York, N.Y.

ATOMIC ENERGY COMMISSION ACTIVITIES

130-132 U.S. Atomic Energy Commission, Technical Library, Washington 25, D.C. ATTN: For LMA
133-134 Los Alamos Scientific Laboratory, Report Library, P.O. Box 1663, Los Alamos, N. Mex. ATTN: Helen Redman
135-139 Sandia Corporation, Classified Document Division, Sandia Base, Albuquerque, N. Mex. ATTN: H. J. Smyth, Jr.
140-149 University of California Lawrence Radiation Laboratory, P.O. Box 808, Livermore, Calif. ATTN: Clovis G. Craig
150 Weapon Data Section, Office of Technical Information Extension, Oak Ridge, Tenn.
151-180 Office of Technical Information Extension, Oak Ridge, Tenn. (Surplus)

Defense Special Weapons Agency
6801 Telegraph Road
Alexandria, Virginia 22310-3398

MAY 8 1998

OPSSI

MEMORANDUM FOR DISTRIBUTION

SUBJECT: Declassification Review of Operation HARDTACK Test Reports

The following 28 reports concerning the atmospheric nuclear tests conducted during Operation HARDTACK in 1958 have been declassified and cleared for open publication/public release:

WT-1606 thru WT-1611, WT-1613 thru WT-1617, WT-1620, WT-1626, WT-1630, WT-1633, WT-1634, WT-1647, WT-1649, ITR-1653, ITR-1655, ITR-1656, WT-1661, WT-1662, WT-1676, WT-1685 thru WT-1687, and WT-1689.

An additional 29 WTs from HARDTACK have been re-issued with deletions and are identified with an "EX" after the WT number. These reissued versions are unclassified and approved for open publication. They are:

WT-1602, WT-1618, WT-1619, WT-1621 thru WT-1623, WT-1625, WT-1627, WT-1629, WT-1636 thru WT-1641, WT-1648, WT-1650, WT-1651-1, WT-1657, WT-1663, WT-1664, WT-1675, WT-1677, WT-1679 thru WT-1682, WT-1688 and WT-1690.

This memorandum supersedes the Defense Special Weapons Agency, OPSSI memorandum same subject dated June 13, 1997 and may be cited as the authority to declassify copies of any of the reports listed in the first paragraph above.

RMetro

RITA M. METRO
Chief, Information Security

DISTRIBUTION:
See Attached